Original Article

U-fiber analysis: a toolbox for automated quantification of U-fibers and white matter hyperintensities

Gaoxing Zheng[1#^], Beini Fei[1#], Anyan Ge[1], Yuchen Liu[2], Ying Liu[1], Zidong Yang[2], Zhensen Chen[2], Xin Wang[1], He Wang[1,2], Jing Ding[1]

[1]Department of Neurology, Zhongshan Hospital, Fudan University, Shanghai, China; [2]Institute of Science and Technology for Brain-inspired Intelligence, Fudan University, Shanghai, China

Contributions: (I) Conception and design: G Zheng, B Fei; (II) Administrative support: X Wang, H Wang, J Ding; (III) Provision of study materials or patients: B Fei, A Ge, Ying Liu; (IV) Collection and assembly of data: A Ge, G Zheng, Yuchen Liu, Z Yang; (V) Data analysis and interpretation: G Zheng, Z Chen, H Wang; (VI) Manuscript writing: All authors; (VII) Final approval of manuscript: All authors.

[#]These authors contributed equally to this work as co-first authors.

Correspondence to: Jing Ding, MD; Xin Wang, MD. Department of Neurology, Zhongshan Hospital, Fudan University, 180 Fenglin Road, Xuhui District, Shanghai 200032, China. Email: ding.jing@zs-hospital.sh.cn; wang.xin@zs-hospital.sh.cn; He Wang, PhD. Institute of Science and Technology for Brain-inspired Intelligence, Fudan University, 220 Handan Road, Yangpu District, Shanghai 200433, China; Department of Neurology, Zhongshan Hospital, Fudan University, 180 Fenglin Road, Xuhui District, Shanghai 200032, China. Email: hewang@fudan.edu.cn

Background: Whether white matter hyperintensities (WMHs) involve U-fibers is of great value in understanding the different etiologies of cerebral white matter (WM) lesions. However, clinical practice currently relies only on the naked eye to determine whether WMHs are in the vicinity of U-fibers, and there is a lack of good neuroimaging tools to quantify WMHs and U-fibers.

Methods: Here, we developed a multimodal neuroimaging toolbox named U-fiber analysis (UFA) that can automatically extract WMHs and quantitatively characterize the volume and number of WMHs in different brain regions. In addition, we proposed an anatomically constrained U-fiber tracking scheme and quantitatively characterized the microstructure diffusion properties, fiber length, and number of U-fibers in different brain regions to help clinicians to quantitatively determine whether WMHs in the proximal cortex disrupt the microstructure of U-fibers. To validate the utility of the UFA toolbox, we analyzed the neuroimaging data from 246 patients with cerebral small vessel disease (cSVD) enrolled at Zhongshan Hospital between March 2018 and November 2019 in a cross-sectional study.

Results: According to the manual judgment of the clinician, the patients with cSVD were divided into a WMHs involved U-fiber group (U-fiber-involved group, 51 cases) and WMHs not involved U-fiber group (U-fiber-spared group, 163 cases). There were no significant differences between the U-fiber-spared group and the U-fiber-involved group in terms of age (P=0.143), gender (P=0.462), education (P=0.151), Mini-Mental State Examination (MMSE) scores (P=0.151), and Montreal Cognitive Assessment (MoCA) scores (P=0.411). However, patients in the U-fiber-involved group had higher Fazekas scores (P<0.001) and significantly higher whole brain WMHs (P=0.046) and deep WMH volumes (P<0.001) compared to patients in the U-fiber-spared group. Moreover, the U-fiber-involved group had higher WMH volumes in the bilateral frontal [P(left) <0.001, P(right) <0.001] and parietal lobes [P(left) <0.001, P(right) <0.001]. On the other hand, patients in the U-fiber-involved group had higher mean diffusivity (MD) and axial diffusivity (AD) in the bilateral parietal [P(left, MD) =0.048, P(right, MD) =0.045, P(left, AD) =0.015, P(right, AD) =0.015] and right frontal-parietal regions [P(MD) =0.048, P(AD) =0.027], and had significantly reduced mean fiber

^ ORCID: 0000-0001-5382-2305.

length and number in the right parietal [P(length) =0.013, P(number) =0.028] and right frontal-parietal regions [P(length) =0.048] compared to patients in the U-fiber-spared group.

Conclusions: Our results suggest that WMHs in the proximal cortex may disrupt the microstructure of U-fibers. Our tool may provide new insights into the understanding of WM lesions of different etiologies in the brain.

Keywords: MATLAB toolbox; U-fiber tractography; white matter hyperintensities (WMHs); cerebral small vessel disease (cSVD); diffusion magnetic resonance imaging (dMRI)

Submitted Jun 13, 2023. Accepted for publication Nov 13, 2023. Published online Jan 02, 2024.
doi: 10.21037/qims-23-847
View this article at: https://dx.doi.org/10.21037/qims-23-847

Introduction

Subcortical U-fibers are special types of short association fibers located in the superficial white matter (SWM). In contrast to the SWM, the U-fibers only connect the adjacent gyri (1-5). Since U-fibers have a rich blood supply from long perforating arteries and short perforating arteries that span the white matter (WM) and adjacent cortex, they are usually unaffected in chronic ischemic WM disease (6,7). Anatomically, U-fibers originate from pyramidal neurons of layer 6 of the cerebral cortex and provide local integration of different sites of the same gyrus or immediately adjacent gyri. Developmentally, U-fibers do not fork until the second half of gestation when gyration and sulcation of the cerebral cortex occur (8-10). As a result, U-fibers are not readily involved in diseases of myelin metabolism, such as adrenoleukodystrophy and metachromatic leukodystrophy (11). However, in demyelinating diseases with normal myelin and oligodendrocyte dominance, including multiple sclerosis and progressive multifocal leukoencephalopathy, U-fibers are commonly involved (12). All evidence suggests that U-fibers contribute to the etiological diagnosis of WM diseases. Quantitative studies of the presence of U-fiber involvement are valuable in narrowing the differential diagnosis of different WM lesions. Recently, several quantitative studies have analyzed disease characteristics and mechanisms based on U-fibers in diseases such as epilepsy (13), autism spectrum disorders (14,15), and first-episode schizophrenia (16). However, in those studies of WM disease, little attention was given to the quantification of U-fibers, especially for cerebral small vessel diseases (cSVD).

To reveal the functional implications of U-fibers, we need to accurately depict the anatomical structures of the WM of the brain. Fiber tracking based on diffusion magnetic resonance imaging (dMRI) represents an excellent technique for understanding the anatomy of the WM in the human brain (17). However, previous studies on WM fiber tracking have focused on fibers in the deep WM (DWM), whereas few studies have investigated U-fibers because of poor anatomical consistency between individuals and the complex arrangement of the superficial gyrus and sulcus (18,19). In addition, U-fibers are located near the border between white and gray matter (WM and GM, respectively), and the fractional anisotropy (FA) values near U-fibers are less consistent for accurately modeling the local fiber orientations during fiber tracking (20). In recent years, advances in dMRI techniques and improved fiber tractography algorithms have made it possible for researchers to study U-fibers (21-26). For example, the multi-shell, multi-tissue constrained spherical deconvolution (MSMT-CSD) algorithm was proposed to improve the fiber orientation estimation at the WM/GM/cerebrospinal fluid (CSF) tissue interface (24). However, few studies have considered the anatomical criteria for U-fibers (i.e., U-fibers are association fibers that connect the adjacent cerebral gyri and travel around the sulcus), resulting in them having tracked superficial WM fibers rather than true U-fibers (4,13). Although researchers are gradually introducing anatomical constraints to obtain U-fibers (27), there is still a lack of easy-to-use open-source tools for clinical applications.

Several studies have shown that lesions of U-fibers can help to distinguish between WM disease of presumed vascular origin and demyelinating WM disease (12,28). In T2-weighted fluid-attenuated inversion recovery (T2 FLAIR) images of patients with demyelinating WM disease, WM hyperintensities (WMHs) are commonly observed involving U-fibers and may cause changes in the dMRI properties of U-fibers (11,29,30). However, in those WM

diseases of presumed vascular origin, WMHs generally do not involve U-fibers due to the presence of blood supply compensation and the relative absence of damage to U-fibers (8,12,31). Currently, there is a lack of appropriate neuroimaging analysis tools to help clinicians determine whether WMH affects U-fiber. Here, we developed a MATLAB toolbox called U-fiber analysis (UFA) to achieve automatic extraction and quantification of U-fibers and WMHs to determine whether WMHs affect U-fibers.

The UFA toolbox has several highlights: (I) it integrates T1W/T2 FLAIR/DWI (diffusion-weighted imaging) multimodal neuroimaging analysis. Users only need to enter the correct path of the original digital imaging and communications in medicine (DICOM) files for automatic pre-processing and post-processing, which is very convenient for clinical applications; (II) it can easily extract detailed WMH volumes and sizes in different brain lobes and arteries; (III) it enables automatic clustering and quantification of different U-fibers, allowing us to observe significant changes in the microstructural features of U-fibers in greater detail, and providing new insights into the onset of disease; (IV) it provides graphics processing unit (GPU) acceleration during DWI preprocessing, reducing the time for eddy current correction. In addition, the FastSurfer tool has been used to accelerate the process of T1 cortical segmentation and surface reconstruction (32). Given the user-friendliness of the tool, it has great potential for clinical use. Finally, it provides quantitative reports including a description of the diffusion measurement of U-fibers, the number and average length of U-fiber bundles, WMH volume and sizes in deep/periventricular regions, and different brain lobes. Our tool currently enables the most detailed quantitative description of U-fibers. We present this article in accordance with the STROBE reporting checklist (available at https://qims.amegroups.com/article/view/10.21037/qims-23-847/rc).

Methods

Participants

A total of 246 participants who underwent a physical examination at Zhongshan Hospital from March 2018 to November 2019 were enrolled in this study. Among them, 26 did not undergo MRI or had MRI image data that was not able to be read using conventional MRI reading software (RadiAnt DICOM Viewer). There was 1 case who had scanned MRI without T1 images. Finally, a total of 219 participants underwent multi-modal MRI scans and were included in the subsequent analysis. An experienced neurologist interpreted MRI images to determine whether WMHs involved U-fibers, blinded to the results of the UFA toolbox. When a patient had more than three lesions involving U-fibers, he/she would be identified in the U-fiber-involved group. A detailed description of the participant information is shown in *Table 1*.

The inclusion criteria were as follows: (I) age between 40 and 70 years; (II) completed cranial MRI scans (including T1W, T2 FLAIR, and DWI); and (III) Fazekas score of no less than 2 (33). The exclusion criteria were as follows: (I) the patient had a pacemaker or other metal implant that prevented MRI scanning; (II) the participant had a serious disease, such as malignancy or severe cardiac insufficiency; (III) participants had a definitive diagnosis of stroke, multiple sclerosis, adrenoleukodystrophy, acute disseminated encephalomyelitis, or a disease with demyelinating changes that may be caused by metabolism or toxicity; (IV) participants had a definite diagnosis of hereditary cSVD (e.g., mitochondrial encephalomyopathy with lactic acidosis and stroke-like episodes (MELAS), cerebral autosomal dominant arteriopathy with subcortical infarcts and leukoencephalopathy (CADASIL), Fabry's disease). This study was approved by the Ethics Committee of Zhongshan Hospital, Fudan University (No. B2018-155) and conducted in accordance with the Declaration of Helsinki (as revised in 2013). All participants provided written informed consent.

MRI examination

All participants received the multi-modal MRI scan using 3T MRI equipment (GE Discovery MR750; GE Healthcare, Chicago, IL, USA), including the T1W scan, T2 FLAIR scan, DWI scan, and other scans [such as blood oxygenation level-dependent (BOLD) imaging, magnetic resonance angiography (MRA), arterial spin labeling (ASL), cerebral blood flow (CBF), time of flight angiography (TOF)] which were not processed in the study. T1W images were scanned with a voxel size of 1 mm × 1 mm × 1 mm by 3-dimensional fast spoiled gradient-echo (3D-FSPGR) sequence (repetition time =7.4 ms, echo time =3.1 ms, 1 mm slice thickness). dMRI data were acquired with a voxel size of 1×1×2, b values of 1,000 and 2,000 s/mm^2 in 30 non-collinear directions with 3 b0 volumes in anterior-posterior (AP) phase encoding direction and 3 b0 volumes

Table 1 Demographic and clinical characteristics of the participants

Characteristics	Total	U-fibers spared	U-fibers involved	Z or chi/P value
Subjects	214	163	51	–
Age, y	56.3±8.0	56.8±8.1	54.8±7.5	1.467/0.143
Female	85 (39.7)	62 (38.0)	23 (45.1)	0.541/0.462
Education, y	9.00±5.00	9.00±5.00	8.50±3.25	1.437/0.151
Hypertension	105 (49.1)	86 (52.8)	19 (37.3)	3.282/0.070
Diabetes mellitus	27 (12.6)	25 (15.3)	2 (3.9)	3.661/0.056
Dyslipidemia	49 (22.9)	39 (23.9)	10 (19.6)	0.221/0.638
MMSE	29±2	29±2	28±1	0.354/0.151
MoCA	24±5	24±6	25±5	–0.823/0.411
Fazekas score	2.5±0.8	2.3±0.7	3.0±1.0	–5.000/<0.001
Lacunes	17 (7.9)	14 (8.6)	3 (5.9)	0.114/0.735
Microbleeds	9 (4.2)	5 (3.1)	4 (7.8)	1.153/0.283
Severe PVS	19 (8.9)	11 (6.8)	8 (15.7)	2.763/0.097
cSVD score	50 (23.4)	32 (19.6)	18 (35.3)	–4.089/<0.001

Data are presented as the absolute numbers (% of total) or mean ± standard deviation. y, year; MMSE, Mini-Mental State Examination; MoCA, Montreal Cognitive Assessment; PVS, perivascular spaces; cSVD, cerebral small vessel disease.

in posterior-anterior (PA) direction. T2 FLAIR resolution was 0.469 mm × 0.469 mm × 0.5 mm.

UFA toolbox framework

The UFA toolbox contains several parts (*Figures 1*,*2*): (I) first, the input folder directory and output folder directory of the single case should be provided. The input folder refers to the multi-modal MRI data folder with each subfolder containing data in DICOM format. (II) Second, the toolbox provides the checkup of three subfolder names (T1/T2 FLAIR/DWI) to ensure the program specifically identifies the unique folder directory. We provide the common matched string of the T1/T2 FLAIR/DWI image folder; if the user finds these strings are not matched with the subfolder name, he/she can choose the bottom of the popup menu 'Input Your Choice' and input the unique folder name. (III) Third, the T1 preprocessing module is provided in the UFA toolbox, including the Gibbs ring artifact removal, bias field correction, tissue segmentation, and registration to DWI b0 image, the detailed description is demonstrated in the 'Data Preprocessing' part of the paper. (IV) Fourth, the DWI preprocessing module and DWI tractography are provided in the toolbox—the DWI preprocessing contains denoise, deGibbs, distortion correction, eddy correction, and bias field correction, and the detailed description is demonstrated in the 'Data Preprocessing' part of the paper. The DWI tractography module takes the MSMT-CSD technique to generate the whole brain WM tractography, the detailed description is provided in the 'DWI Tractography' part of the paper. (V) Fifth, the T2 FLAIR WMH extraction module is provided in the toolbox—it calls the unidentified bright objects detector (UBO Detector) toolbox to automatically extract the WMH and finally gives the quantified description of WMH volume and counts. (VI) Sixth, the UFA module is provided in the toolbox—it includes U-fiber filtering part, U-fiber clustering part, and U-fiber quantification part. In the U-fiber filtering part, we provided the 'length filter', 'U shape filter', 'superficial filter', and 'gyrus-gyrus filter' 4 choices to automatically generate the U-fiber tractography. In the U-fiber clustering part, we adopt the WM analysis (WMA) tool developed by O'Donnell's group to cluster the fibers into 800 clusters (containing 198 superficial clusters) and group them into 16 superficial tracts. In the U-fiber quantification part, the average length and number of 16 U-fiber tracts were provided. Moreover, we provide the diffusion tensor metrics [such as FA/mean

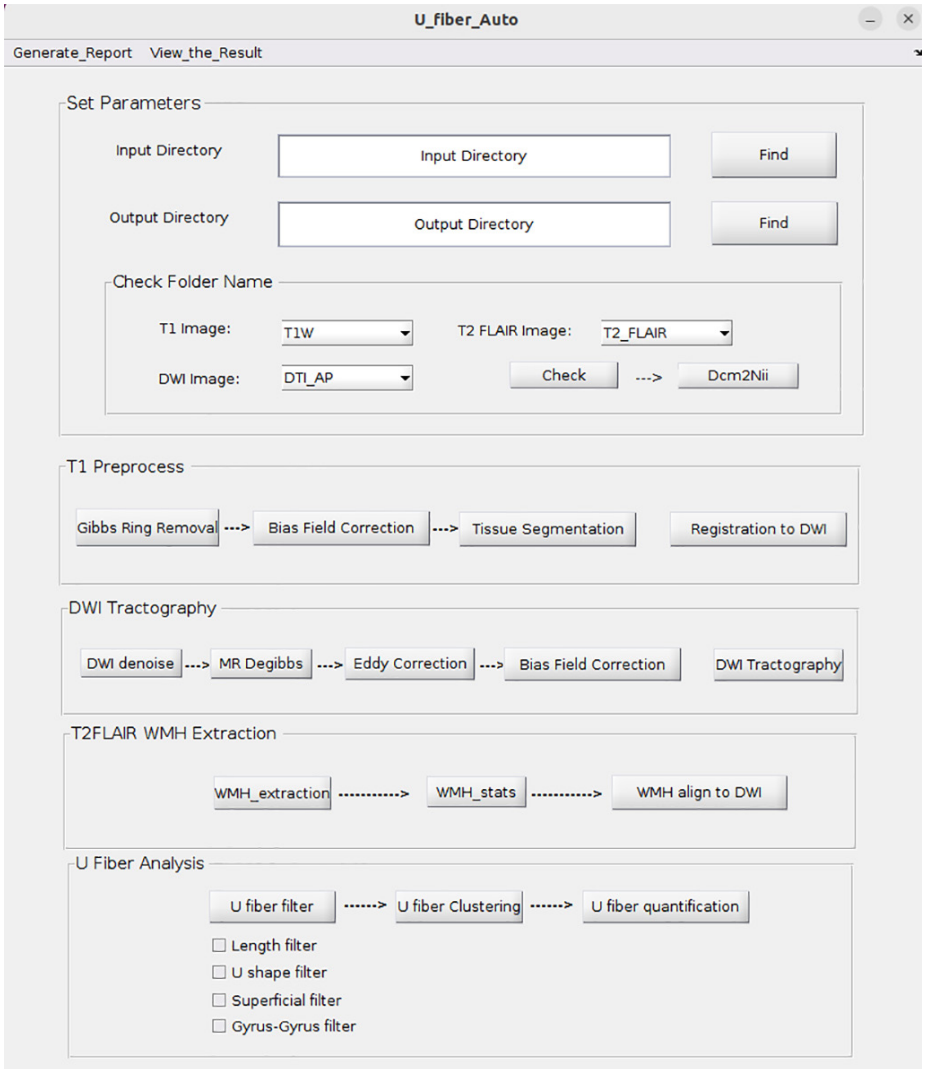

Figure 1 The GUI of the UFA toolbox. GUI, Graphical User Interface; UFA, U-fiber analysis; T1W, T1-weighted image; FLAIR, fluid-attenuated inversion recovery; DTI, diffusion tensor imaging; AP, anterior-posterior; DWI, diffusion-weighted imaging; MR, magnetic resonance; WMH, white matter hyperintensity.

diffusivity (MD)/axial diffusivity (AD)/radial diffusivity (RD)] of the 16 U-fibers tracts. The UFA toolbox can be acquired from Baidu Netdisk (link: https://pan.baidu.com/s/1nSwxoQtRrrbeiO3-bQis0w; password: v9uw) or Github (https://github.com/GaoxingZheng/UFA_toolbox). A step-by-step video demonstration of the correct use of the UFA toolbox can be found (*Video 1*).

Data preprocessing

Each T1W image was preprocessed by several steps. Firstly, The Gibbs artifact was removed (34) and then the bias field was corrected by using advanced normalization tools (35,36) (*Figures 1*,*2B*,*2E*). Then, the T1W image was segmented into GM/subcortical GM/WM/CSF and pathological tissue by using the MRtrix3 command '5ttgen' (37). Each DWI image was preprocessed by several steps (23). Firstly, the 'dwidenoise' command was used to denoise the diffusion MRI image (38). Secondly, the Gibbs artifact was removed by using the MRtrix3 command 'mrdegibbs' (34). Thirdly, the MRtrix3 command 'dwifslpreproc' was applied for eddy correction (39-43), in which 1 b0 image in the AP phase encoding direction and one b0 image in the PA direction were merged into a paired b0 image by the command

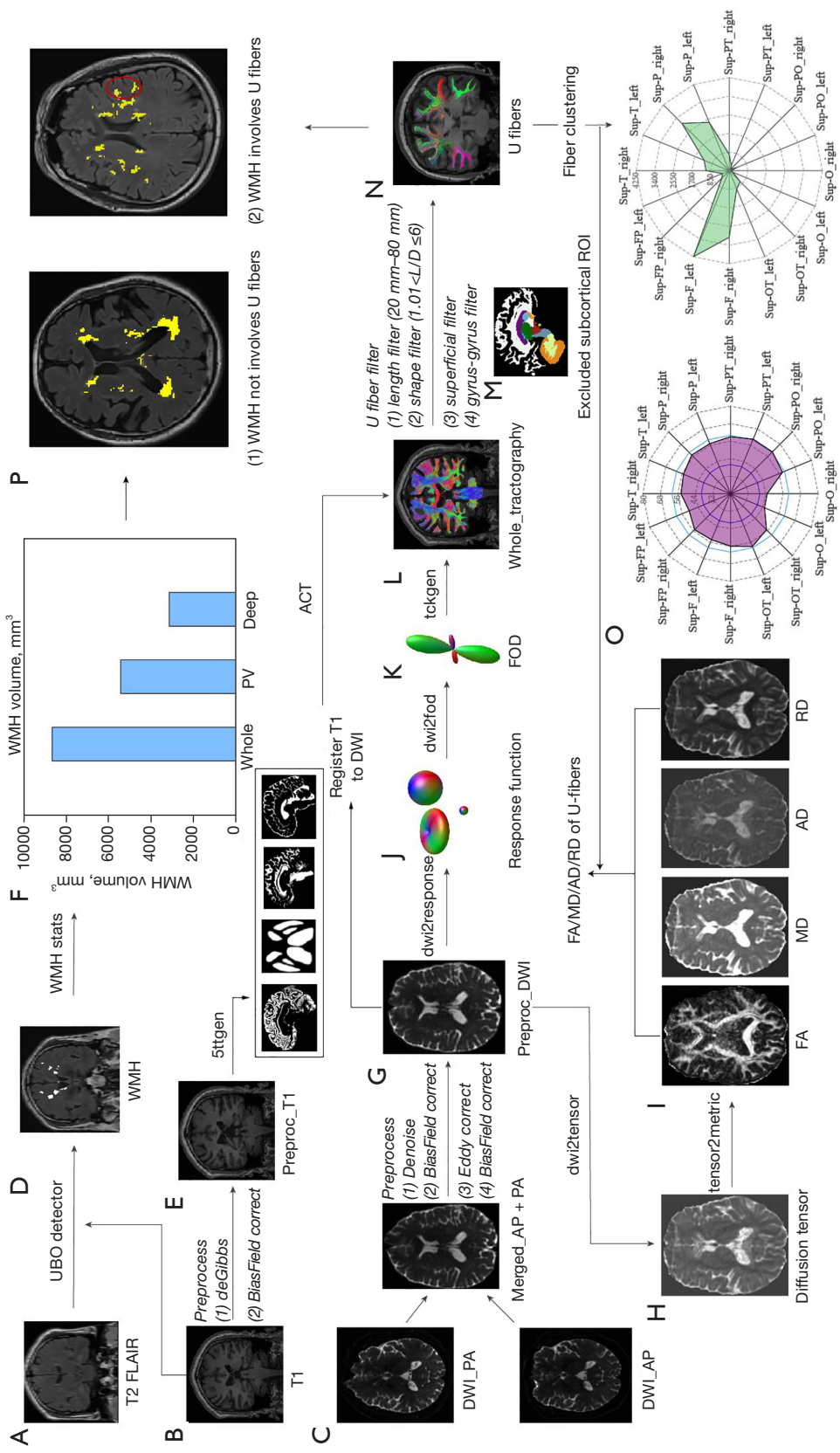

Figure 2 Multimodal MRI data preprocessing and post-processing pipeline provided by the UFA toolbox. cSVD patient's (A) T2 FLAIR image; (B) T1 image; and (C) DWI image with two phase encoding directions (DWI_AP, DWI_PA), AP indicates the anterior-posterior phase encoding direction and PA indicates the posterior-anterior phase encoding direction; (D) WMHs image after extraction by UBO Detector open source tool, white dots indicate WMHs extracted by the algorithm; (E) preprocessed T1 image; (F) schematic diagram of whole brain/periventricular/deep WMHs volume; (G) preprocessed DWI image; (H) diffusion tensor image obtained by diffusion tensor modeling of DWI image; (I) four diffusion metrics (FA/MD/AD/RD); (J) response function diagram of three tissues (gray matter/white matter/cerebrospinal fluid) in DWI image; (K) schematic of local fiber orientation distribution; (L) schematic of whole brain white matter fiber bundles; (M) schematic of subcortical gray/white matter ROI for exclusion of deep white matter fiber bundles passing through ROI; (N) schematic of U fibers; (O) schematic of mean fiber length (26) and fiber number (right) of 16 U fibers; (P) schematic diagrams of WMHs not involving U fibers (26) and involving U fibers (right); red circle represents WMHs with U-fiber involvement. cSVD, cerebral small vessel disease; T2 FLAIR, T2-weighted fluid-attenuated inversion recovery; DWI, diffusion-weighted imaging; AP, anterior-posterior; PA, posterior-anterior; WMHs, white matter hyperintensities; PV, periventricular; UBO, unidentified bright objects; FA, fractional anisotropy; MD, mean diffusivity; AD, axial diffusivity; RD, radial diffusivity; ROI, region of interest; ACT, anatomically-constrained tractography; Sup-F, superficial-frontal; Sup-FP, superficial-frontal-parietal; Sup-O, superficial-occipital; Sup-OT, superficial-occipital-temporal; Sup-P, superficial-parietal; Sup-PO, superficial-parietal-occipital; Sup-PT, superficial-parietal-temporal; Sup-T, superficial-temporal.

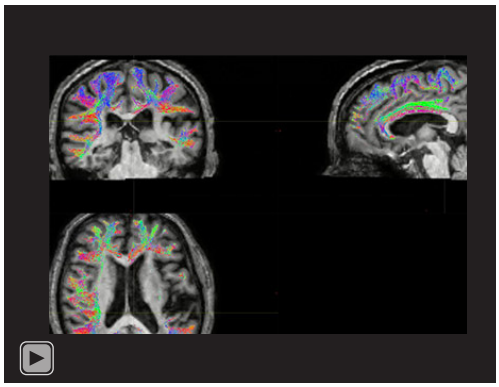

Video 1 Video demonstration of how to use the UFA toolbox. UFA, U-fiber analysis.

'mrcat'. Finally, the N4 bias field was used to correct the preprocessed DWI image.

After the preprocessing, the T1W image was registered to DWI b0 image. The registration procedure was as follows: (I) DWI b0 image was first registered to T1W brain image (without skull) by using the FMRIB software library (FSL) command 'flirt' and generating the initial transform matrix (44,45); (II) DWI b0 image was registered into preprocessed T1W image by using 'flirt' and boundary-based registration (BBR) registration (46) and generated the transform matrix (dwi2T1.mat); (III) The inverse transform matrix (T12dwi.mat) was generated by using command 'convert_xfm'; (IV) T1W image was finally registered into DWI b0 image by using the command 'mrtransform'.

DWI tractography

In this paper, the multi-shell, multi-tissue constrained spherical deconvolution technique was adopted to model the local fiber orientation distribution (24). First, the MRtrix3 command 'dwi2response' was used to generate the response kernel function of GM, WM, and CSF (47). Then, the MRtrix3 command 'dwi2fod' was used to estimate the local fiber orientation distributions (21,22). Next, the MRtrix3 command 'tckgen' was used to generate the whole brain WM fiber tractography. Here, we provide 5 tissue segmentations images as the anatomical constraint during fiber tracking and the second-order integration over fiber orientation distributions (iFOD2) algorithm was used for fiber tracking (48). Of course, users can manually modify the source code of the UFA toolbox to select other algorithms (such as iFOD1). As for the parameters set in the 'tckgen' command, the maximum angle in degree was set as 45 in the study, the minimum fiber length was set as 4 mm (2 × voxel size), the maximum fiber length was set as 200 mm (100 × voxel size), and the total number of fibers was set as 1 million (1M).

Quantification of WMHs

In the WMH automatic extraction part, we wrote MATLAB interface codes of UBO Detector (49-51) so that the UFA can automatically call the codes of UBO Detector to automatically extract WMH and calculate the volume and counts of WMH in different brain lobes and arteries (*Figures 2F,3*, Figure S1). UBO Detector is an open-source neuroimaging tool developed by the Centre for Healthy Brain Ageing (CHeBA) team at the University of New South Wales (UNSW), Australia, which mainly utilizes the k-nearest neighbor algorithm (k-NN) to achieve automatic extraction of WMHs. It takes the T1-weighted image and the T2 FLAIR image as input and completes the preprocessing by using statistical parametric mapping 12 (SPM12) and FSL. Then, the FMRIB's automated segmentation tool (FAST) algorithm was used to generate the candidate categories. Subsequently, the k-NN algorithm was used to judge whether the candidate categories should be divided into WMHs or not.

U-fiber filtering

The UFA toolbox can automatically generate U-fiber tractography from the whole WM tractography by using 4 filtering conditions. The 4 filtering conditions are as follows: (I) length filter, the length of U-fiber usually ranges from 20 and 80 mm (4), therefore, we kept the fibers with lengths that met the conditions and removed those with lengths that did not meet the conditions; (II) U-shape filter, U-fibers are shaped like U-shape curves, the fiber streamline of U-shape usually meet the requirements in which the fiber length (L) divided by endpoints distance (D) ranges from 1.01 to 6; (III) superficial filter, the U-fibers are located in the superficial WM regions, so we automatically remove the fibers passing the DWM regions by using the MRtrix3 command 'tckedit'. The deep cortical WM regions of interest (ROIs) were generated as follows: First, we generated the anatomical segmentation and cortical parcellation of the T1 image based on the Destrieux atlas provided by Freesurfer. Then, we generated the corresponding deep GM or WM ROIs (e.g., corpus callosum, thalamus, hippocampus, amygdala, caudate,

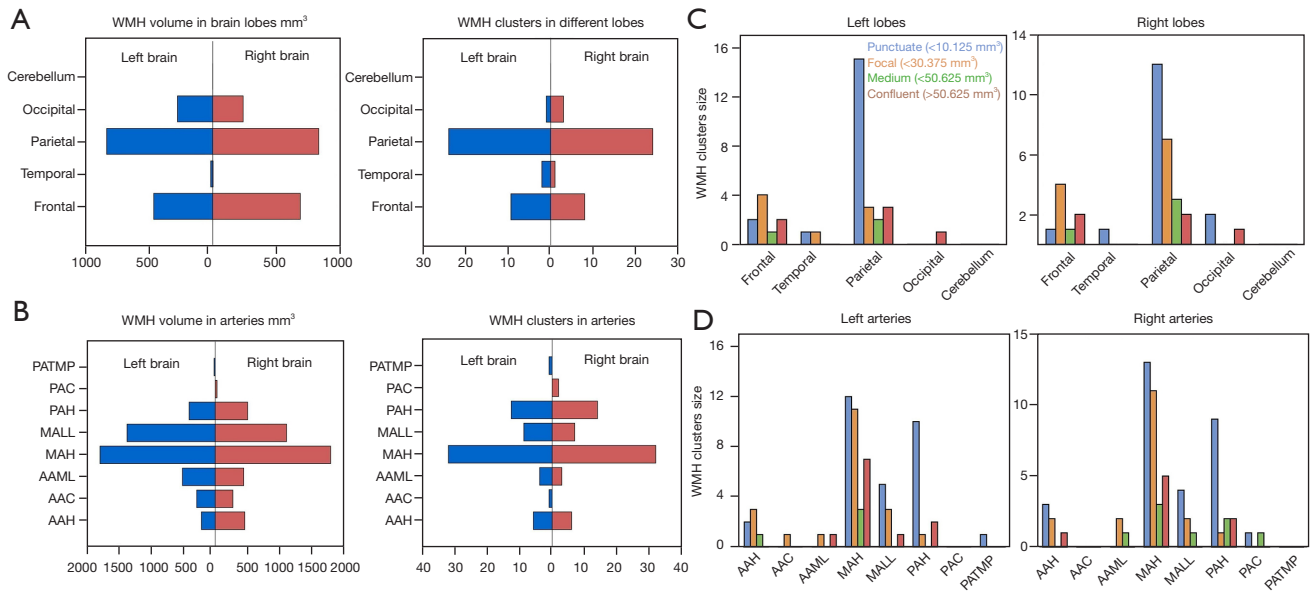

Figure 3 Visualization examples of WMHs in different brain lobes and different arterial territories provided by the UFA toolbox. (A) WMH volume (left panel) and WMH clusters (right panel) in different brain lobes; (B) WMH volume (left panel) and WMH clusters (right panel) in different arteries; (C) four types of WMH clusters (punctuate, focal, medium, confluent) in different brain lobes (left lobes in the left panel, right lobes in the right panel); (D) four types of WMH clusters (punctuate, focal, medium, confluent) in different arteries (left arteries in the left panel, right arteries in the right panel). WMHs, white matter hyperintensities; UFA, U-fiber analysis; AAH, anterior artery hemisphere; AAC, anterior artery callosal; AAML, anterior artery medial lenticulostriate; MAH, middle artery hemisphere; MALL, middle artery lateral lenticulostriate, PAH, posterior artery hemisphere; PAC, posterior artery callosal; PATMP, posterior artery thalamic and midbrain perforators.

putamen, etc.) based on the Destrieux atlas lookup table and these segmentations. If the fibers passed through these deep ROIs, they were removed and finally we obtained the superficial fibers. It is worth noting that we accelerated the progress of T1 segmentation and surface reconstruction by using FastSurfer (32,52). FastSurfer is a fast tissue segmentation and surface reconstruction tool based on fast-convolutional neural network (fast-CNN). Compared with FreeSurfer (53), FastSurfer can greatly reduce the running time of cortical tissue segmentation, which is very suitable for clinical application. (IV) Gyrus-gyrus filter, the U-fibers connect the neighbored gyri and travel around the sulcus (1). Here we use the gyri labeling method similar to Schilling *et al.* (54) to generate 82 paired adjacent gyri using the Destrieux atlas (Table S1) (55). If the start point of the fiber streamlines is in a certain gyrus and the end point is in the adjacent gyrus, then the streamline is reserved to obtain the U-fibers, otherwise, the streamline is eliminated.

U-fiber clustering and quantification

In the U-fiber clustering module, we wrote codes to interface the UFA toolbox with the WMA tool to cluster and quantify U-fibers. The WMA tool was developed by the O'Donnell Research Group (ORG) and is easily used for fiber clustering and visualization (56-59). The ORG created a WM atlas of 800 clusters based on data from 100 young adult cases from the Human Connectome Project (HCP) dataset. The clustering process of the WMA tool consists of 4 main steps (Figure S2): first, a quality control code is performed to check whether the bundle anatomy coordinate system is the same as the ORG 800-atlas; second, the WM tractography generated by the UFA toolbox is registered to the ORG atlas; third, a fiber clustering procedure is performed and the outliers are removed to filter false positive fibers; and finally, the 800 clusters are converted to the original space and categorized into left, right and

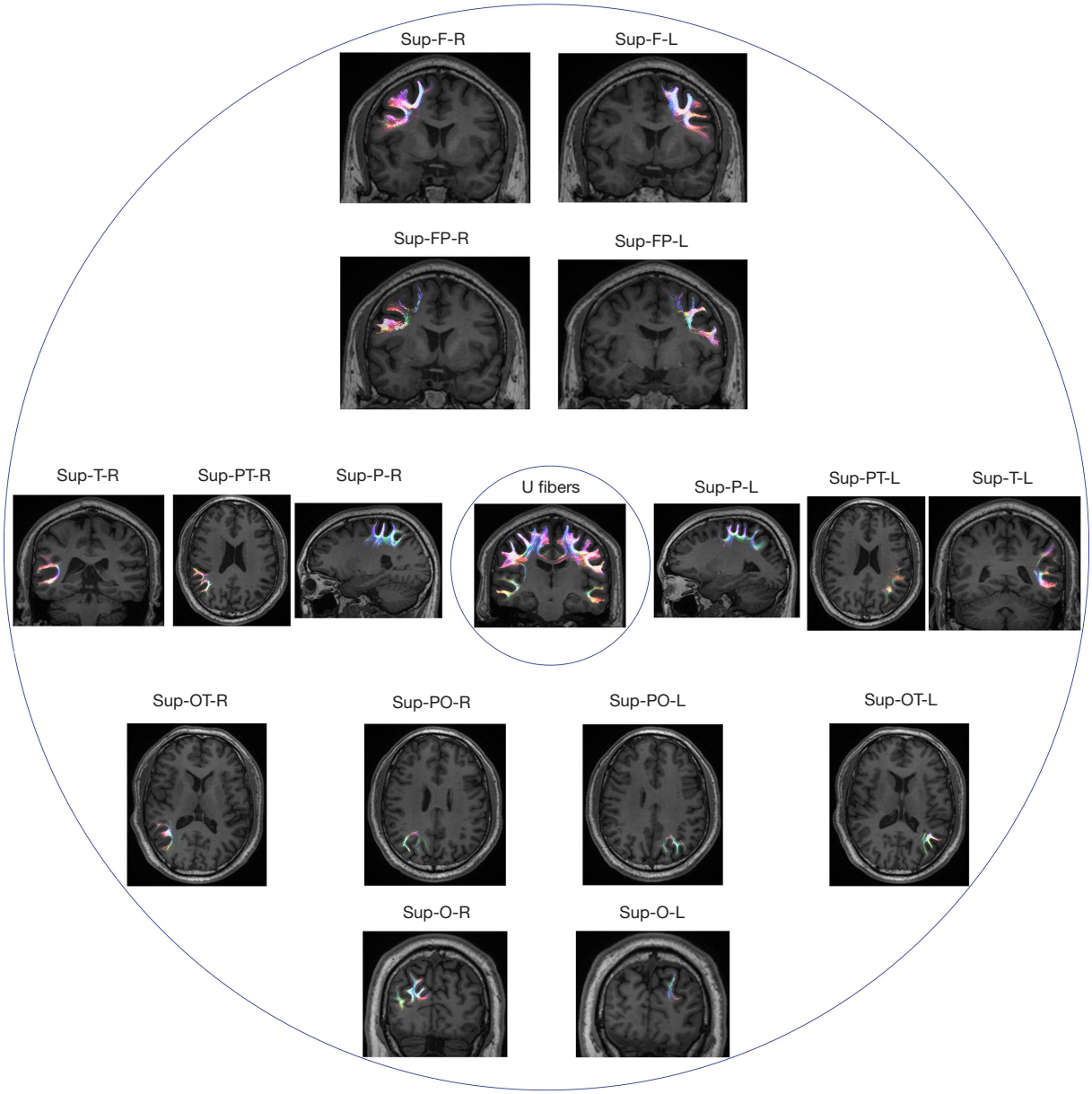

Figure 4 The 16 U-fiber clusters provided in the ORG atlas in the WMA tool. ORG, O'Donnell Research Group; WMA, white matter analysis; L, left hemisphere; R, right hemisphere; Sup-F, superficial-frontal; Sup-FP, superficial-frontal-parietal; Sup-O, superficial-occipital; Sup-OT, superficial-occipital-temporal; Sup-P, superficial-parietal; Sup-PO, superficial-parietal-occipital; Sup-PT, superficial-parietal-temporal; Sup-T, superficial-temporal.

commissural tracts.

In the UFA toolbox, we were interested in the U-fiber clusters and therefore considered the 16 superficial clusters in the ORG atlas in the subsequent U-fiber quantification (*Figure 4*). We calculated the average length and number of the 16 U-fiber bundles to compare significant differences between groups. In addition, to evaluate the microstructural changes of the U-fibers in the WM, we calculated the diffusion tensor metrics (FA/MD/AD/RD) for the 16 U-fiber bundles. The computational steps were as follows: first, we calculated the diffusion tensor metrics of the whole WM; second, we generated the 16 U-fiber bundles; finally, we obtained the diffusion tensor metrics of each U-fiber by masking the U-fiber tractography into the whole brain

diffusion tensor map.

Statistical analysis

All statistical analyses were performed using MATLAB R2019b (The MathWorks Inc., Natick, MA, USA). The Shapiro-Wilk test was used to assess whether the data followed a normal distribution. The 2-sample F-test (MATLAB function 'vartest2') was used to test whether the variance between the two groups was equal. For data that did not follow a normal distribution (such as WMHs), log transformation was used and the 2-sample *t*-test (MATLAB function 'ttest2') was used to assess the difference between the two groups. For those data that still did not conform to normal distribution after conventional transformation, a non-parametric test (Wilcoxon rank sum test) was used to assess whether the difference between the two groups was significant. For missing data, not a number (NaN) was used to replace the specific value. For parametric tests, the mean and standard deviation (SD) of the two groups were reported. For nonparametric tests, medians and interquartile ranges (IQR) were reported for the two groups. In this study, 2-tailed tests were used and a P value of less than 0.05 was considered significant.

Results

Multi-modal neuroimaging analysis results provided by UFA toolbox

Our UFA toolbox provides an integrated solution for multimodal neuroimaging pre-processing and post-processing (*Figure 2*). Firstly, the tool is very convenient for the extraction and quantification of WMHs, and the users can easily calculate the volume and number of WMHs in different brain regions, different brain lobes, and different arterial territories (*Figure 3*). Secondly, the toolbox provides a U-fiber filtering module and a fiber clustering module (Figure S2, *Figure 4*), so users can extract U-fiber bundles and quantify the microstructural diffusion metrics (FA/MD/AD/RD) (*Figure 5*), the average fiber length, and the number of fibers in different superficial brain regions for U-fibers. Furthermore, our toolbox provides many visualization modules, such as WMHs visualization (Figure S3), U-fiber visualization (Figure S4), U-fiber clustering visualization (Figure S5), and WMHs overlap U-fiber visualization for clinicians (Figure S6). Moreover, our toolbox provides 1-click automated data analysis reports in Microsoft 'word' format to facilitate a review of the analysis results (Figure S7).

Running time comparison of UFA toolbox in two computer configurations

In order to successfully use the UFA toolbox, we first need to install the toolkits listed in *Table 2* on Ubuntu. The technical details of how to install these toolkits and successfully use the UFA toolbox have been explained in the tutorial. We deployed the UFA toolbox in 2 computer configurations (*Table 3*) and compared the running time of each step in both configurations (*Table 4*). The first configuration includes a desktop computer with an 11th generation Intel i7-11700 central processing unit (CPU) processor with 8 CPU cores, 64 G of running memory, and a GeForce RTX 3080Ti graphic card with 10G memory. The second computer configuration contains a 12th-generation Intel i7-12700K processor with 12 CPU cores, 64 G of running memory, and a GPU with 10 G memory (GeForce RTX 3080).

Overall, the UFA toolbox in the second computer configuration took significantly less time to complete all pre-processing and post-processing than the first computer configuration (5.120 *vs.* 6.466 hours). The longest processing time was required for the U-fiber filtration step in both configurations: 3.733 hours in the first computer configuration and 2.481 hours in the second computer configuration. In addition, the UFA toolbox also took more than half an hour to compute the single steps of U-fiber clustering, whole brain WM tracking, and DWI image eddy current correction (*Table 4*). Notably, although the total running time for T1W/T2 FLAIR/DWI neuroimaging analysis for a single subject is still a bit long, the time for the DWI eddy correction step and the T1 cortical and surface reconstruction steps has been greatly reduced by using the compute unified device architecture (CUDA) acceleration module.

Demographic and clinical characteristics of the U-fiber-spared group and U-fiber-involved group

Out of a total of 219 cSVD patients who underwent T1W/T2 FLAIR/DWI scans, 2 failed to track whole brain WM fibers, and 2 failed to extract WMHs due to the poor image quality. Therefore, we successfully extracted WMHs and performed U-fibers tracking and quantification in 215 cases (*Figure 6*).

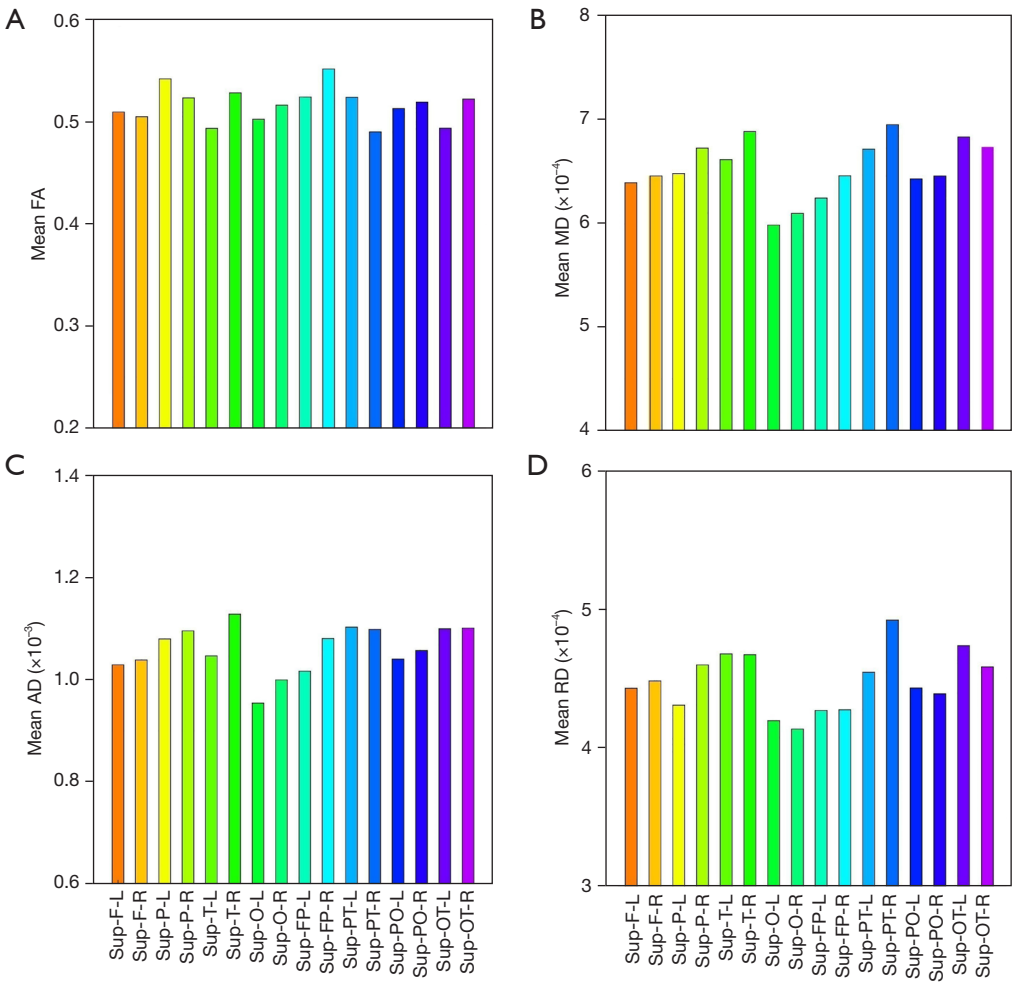

Figure 5 Visualization of diffusion microstructure parameters (FA/MD/AD/RD) in 16 superficial white matter tracts. FA, fractional anisotropy; MD, mean diffusivity; AD, axial diffusivity; RD, radial diffusivity; L, left hemisphere; R, right hemisphere; Sup-F, superficial-frontal; Sup-P, superficial-parietal; Sup-T, superficial-temporal; Sup-O, superficial-occipital; Sup-FP, superficial-frontal-parietal; Sup-PT, superficial-parietal-temporal; Sup-PO, superficial-parietal-occipital; Sup-OT, superficial-occipital-temporal.

Table 2 A list of neuroimaging toolbox required for successful use of the UFA toolbox

Toolbox	Website	Platform	Usage
CNS	https://github.com/cheba-nil/CNS	MATLAB	WMH extraction
SPM12	https://www.fil.ion.ucl.ac.uk/spm/software/spm12/	MATLAB	Required by CNS toolbox
FSL	https://fsl.fmrib.ox.ac.uk/fsl/fslwiki	–	Registration module in FSL 'flirt'
ANTs	http://stnava.github.io/ANTs/	–	N4 bias field correction in ANTs are needed
FastSurfer	https://github.com/Deep-MI/FastSurfer	Python	T1 cortical segmentation
WMA	https://github.com/SlicerDMRI/whitematteranalysis	Python	White matter fiber clustering
3D Slicer	https://www.slicer.org/	Linux version	Required by WMA tool
FreeSurfer	https://surfer.nmr.mgh.harvard.edu/	–	T1 cortical segmentation
MRtrix3	https://www.mrtrix.org/	Linux version	dMRI tractography

UFA, U-fiber analysis; CNS, CHeBA NiL Software; WMH, white matter hyperintensity; SPM12, Statistical Parametric Mapping version 12; FSL, FMRIB Software Library; ANTs, advanced normalization tools; WMA, white matter analysis; dMRI, diffusion magnetic resonance imaging.

Table 3 Software and hardware configurations required for the accelerate calculation

Configuration	Release version	Detailed information	Version number	Categories
Configuration 1	CPU	11th Gen Intel(R) Core(TM) i7-11700@2.50 GHz (Number of CPUs: 1; CPU cores: 8)	–	Hardware
	Running memory	63,986 M (≈64 G)	–	–
	Ubuntu	https://releases.ubuntu.com/20.04/	20.04.4	Operating system
	GPU	GeForce RTX 3080 Ti (GPU memory: 9984 M≈10 G)		Accelerate hardware
	PYTHON	https://www.python.org/	3.8.12	Software
	MATLAB	https://matlab.mathworks.com/	R2019b	Software
	CUDA	https://developer.nvidia.com/cuda-10.2-download-archive?target_os=Linux	v10.2.89	Accelerate module
	NVIDIA Driver	https://www.nvidia.com/download/driverResults.aspx/188877/en-us	470.129.06	Accelerate module
Configuration 2	CPU	12th Gen Intel (R) Core (TM) i7-12700K (Number of CPUs: 1; CPU cores: 12)	–	Hardware
	Running memory	64070 M (≈64 G)	–	–
	Ubuntu	https://releases.ubuntu.com/22.04/	22.04.04	Operating system
	GPU	GeForce RTX 3080 (GPU memory: 10240 M≈10 G)	–	Accelerate hardware
	PYTHON	https://www.python.org/	3.9.12	Software
	MATLAB	https://matlab.mathworks.com/	R2019b	Software
	CUDA	https://developer.nvidia.com/cuda-downloads	v11.7.99, v10.2.89	Accelerate module
	NVIDIA Driver	https://www.nvidia.com/Download/index.aspx	515.65.01	Accelerate module

CPU, central processing unit; GPU, graphics processing unit; CUDA, compute unified device architecture.

Based on the visual judgment of one experienced physician, the 215 participants were divided into 2 groups: the U-fiber-involved group (51 cases) and the U-fiber-spared group (163 cases). The remaining 1 case had other brain lesions and did not belong to either group. There were no significant differences in age (P=0.143), gender (P=0.462), education level (P=0.151), Mini-Mental State Examination (MMSE) scores (P=0.151), and Montreal Cognitive Assessment (MoCA) scores (P=0.411) between the U-fiber-spared group and U-fiber-involved group (*Table 1*). However, the Fazekas score was higher in the U-fiber-involved group than in the U-fiber-spared group (P<0.001), implying a greater burden of WMHs in the U-fiber-involved group.

Higher WMHs burden in the U-fiber-involved group than in the U-fiber-spared group

Compared with the U-fiber-spared group (*Figure 7A*), the cases in the U-fiber-involved group showed significantly higher WMH volume in the whole brain [mean ± SD: 7.39±9.13 *vs.* 9.74±12.03 cm^3, t(212)=2.006, P=0.046, Cohen's d =0.322] and in the DWM region [2.49±3.08 *vs.* 4.46±4.43 cm^3, t(212)=3.650, P<0.001, Cohen's d =0.586]. No significant differences were found in WMH volumes in the periventricular (PV) region between the 2 groups [t(212)=0.757, P=0.450, Cohen's d =0.121].

When we analyzed the WMH volume for different brain lobes and the cerebellum (*Figure 7B*), we found that the U-fiber involved group showed significantly higher WMH volume than the U-fiber-spared group in the bilateral frontal [left lobe: 0.34±0.37 *vs.* 0.68±0.71 cm^3, t(212)=5.784, P<0.001, Cohen's d =0.928; right lobe: 0.27±0.36 *vs.* 0.69±0.72 cm^3, t (210)=6.392, P<0.001, Cohen's d =1.026] and parietal lobes [left lobe: 0.47±0.61 *vs.* 0.90±1.58 cm^3, t(212)=3.391, P<0.001, Cohen's d =0.544; right lobe: 0.43±0.62 *vs.* 0.83±1.13 cm^3, t(212)=3.667, P<0.001 , Cohen's d =0.588].

Table 4 Comparison of pre-processing and post-processing running time of the same subject using UFA toolbox under different computer configurations

UFA module	Each step of UFA toolbox	Running time (configuration 1)	Running time (configuration 2)
Dcm2Nii	DWI AP	3.489 s	4.701 s
	DWI PA	0.528 s	0.679 s
	T1	0.222 s	0.291 s
	T2 FLAIR	0.057 s	0.128 s
T1	Gibbs ring removal	3.604 s	2.321 s
	Bias field correction and ANTs brain extraction	374.080 s (≈6.237 min)	1,884.024 s (≈31.400 min)
	True segmentation	277.991 s (≈4.633 min)	235.434 s (≈3.924 min)
	Registration to DWI	85.598 s (≈1.427 min)	64.229 s (≈1.070 min)
DWI tractography	DWI denoise	48.269 s	38.797 s
	MR deGibbs	29.552 s	18.131 s
	Eddy correction	1,804.674 s (≈30.078 min)	1,501.712 s (≈25.029 min)
	Bias field correction	45.201 s	81.966 s (≈1.366 min)
	DWI tractography	2,395.709 s (≈39.928 min)	1,471.480 s (≈24.525 min)
T2 FLAIR WMH extraction	WMH extraction	154.115 s (≈2.569 min)	122.568 s (≈2.043 min)
	WMH stats	16.448 s	14.718 s
	WMH align to DWI	165.469 s (≈2.758 min)	121.839 s (≈2.031 min)
UFA	U-fiber filtering	13,439.303 s (≈3.733 h)	8,931.125 s (≈2.481 h)
	U-fiber clustering	4,420.568 s (≈1.228 h)	4254.574 s (≈1.182 h)
	U-fiber quantification	12.527 s	7.245 s
Total running time		23,277.404 s (≈6.466 h)	18,755.962 s (≈5.120 h)

UFA, U-fiber analysis; DWI, diffusion-weighted imaging; AP, anterior-posterior; PA, posterior-anterior; FLAIR, fluid-attenuated inversion recovery; ANTs, advanced normalization tools; MR, magnetic resonance; WMHs, white matter hyperintensities.

When we analyzed the WMH volume in different arterial territories (*Figure 7C*), we found that the U-fiber involved group showed significantly higher WMH volume than the U-fiber spared group in the bilateral anterior artery hemisphere (AAH) [left AAH: 0.18±0.26 *vs.* 0.38±0.41 cm^3, t(212)=4.509, P<0.001, Cohen's d =0.723; right AAH: 0.19±0.32 *vs.* 0.42±0.45 cm^3, t(212)=3.915, P<0.001, Cohen's d =0.628], bilateral middle artery hemisphere (MAH) [left MAH 1.38±1.86 *vs.* 1.97±2.86 cm^3, t(212)=3.019, P=0.003, Cohen's d =0.484; right MAH 1.30±1.97 *vs.* 1.83±2.47 cm^3, t(212)=3.095, P=0.002, Cohen's d =0.497] and right posterior artery callosal (PAC) [0.003±0.010 *vs.* 0.003±0.017 cm^3, t(108)=2.170, P=0.032, Cohen's d =0.487].

Differences in U-fiber diffusion metrics in different brain regions between the U-fiber-involved group and U-fiber-spared group

The FA of U-fibers in different brain regions did not differ significantly between U-fiber-involved group and the U-fiber-spared group (*Figure 8A*). The MD of the U-fiber-involved group was significantly higher than those in U-fiber-spared group in the bilateral parietal regions [left region: 0.68±0.05 *vs.* 0.69±0.06 μm^2/ms, t(212)=1.987, P=0.048, Cohen's d =0.319; right region: 0.68±0.05 *vs.* 0.69±0.05 μm^2/ms, t(212)=2.019, P=0.045, Cohen's d =0.324] and right frontal-parietal region [0.67±0.05 *vs.*

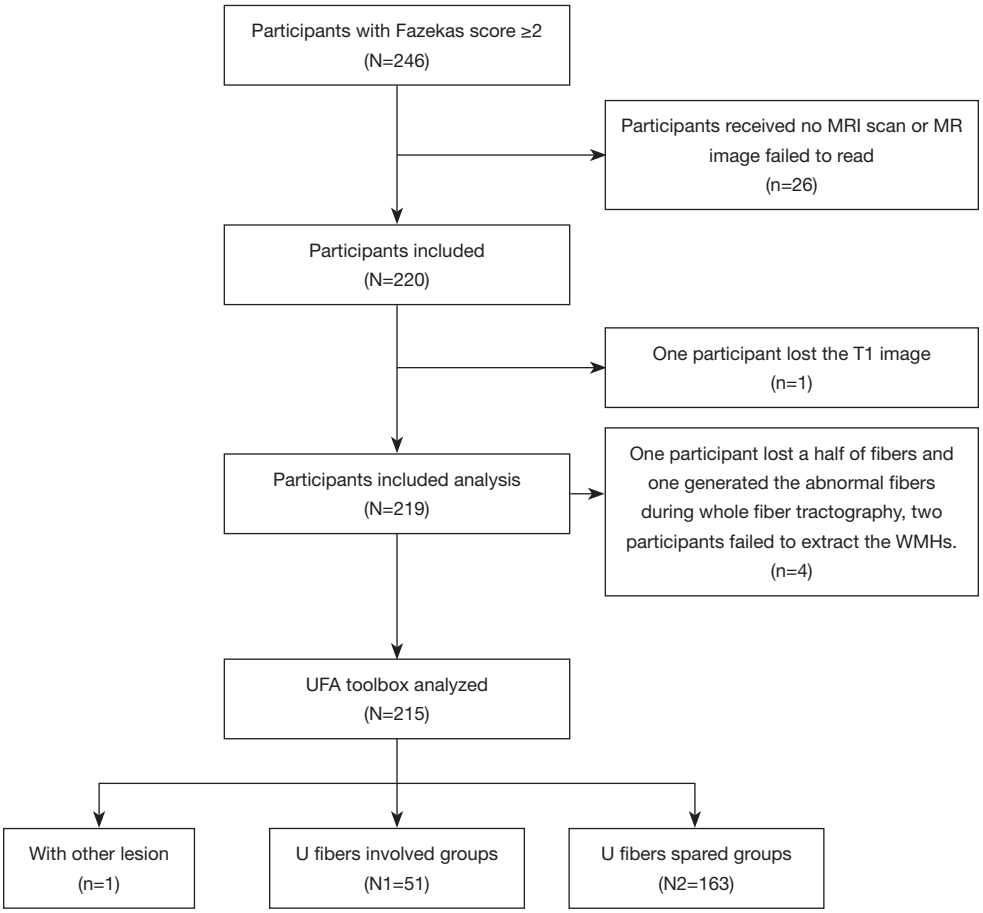

Figure 6 Inclusion and exclusion flowchart of cSVD participants. Finally, 51 subjects with U-fibers involved and 163 subjects with U-fibers spared were analyzed by our UFA toolbox. MRI, magnetic resonance imaging; WMHs, white matter hyperintensities; cSVD, cerebral small vessel disease; UFA, U-fiber analysis.

0.69±0.06 μm^2/ms, t(212)=1.990, P=0.048, Cohen's d =0.319] (*Figure 8B*). The AD of U-fibers-involved group were significantly higher than in the U-fiber spared group in the bilateral parietal regions [left region: 1.10±0.09 *vs.* 1.10±0.08 μm^2/ms, t(212) =2.465, P=0.015, Cohen's d =0.396; right region: 1.10±0.08 *vs.* 1.10±0.08 μm^2/ms, t(212)=2.447, P=0.015, Cohen's d =0.393] and right frontal-parietal region [1.10±0.08 *vs.* 1.10±0.07 μm^2/ms, t(212)=2.235, P=0.027, Cohen's d =0.359] (*Figure 8C*). The RD did not show significant differences between the two groups (*Figure 8D*).

The mean fiber length of the U-fiber-involved group was significantly shorter than that of the U-fiber-spared group in the right parietal region [41.84±3.32 *vs.* 40.88±2.81, t(212)=−2.519, P=0.013, Cohen's d =−0.404] and right frontal-parietal region [42.18±4.35 *vs.* 40.41±4.44, t(212)=−1.987, P=0.048, Cohen's d =−0.319] (*Figure 9A*). The mean fiber counts of the U-fiber-involved group were also significantly lower than those in the U-fiber-spared group in the right parietal region [22,004±542 *vs.* 20,204±626, t(212)=−2.211, P=0.028, Cohen's d =−0.355] (*Figure 9B*).

Discussion

In this paper, we developed a multi-modal neuroimaging analysis toolbox named UFA to help clinicians to explore the clinical value of U-fibers. One of the advantages of the UFA is that it provides an integrated T1W/T2 FLAIR/DWI image analysis pipeline, which will enable clinicians to use information from multiple modalities to comprehensively assess brain WM lesions. Another advantage is that we use GPU acceleration, which greatly reduces the computation time of some modules (e.g., eddy current correction of dMRI, T1 cortex segmentation, and

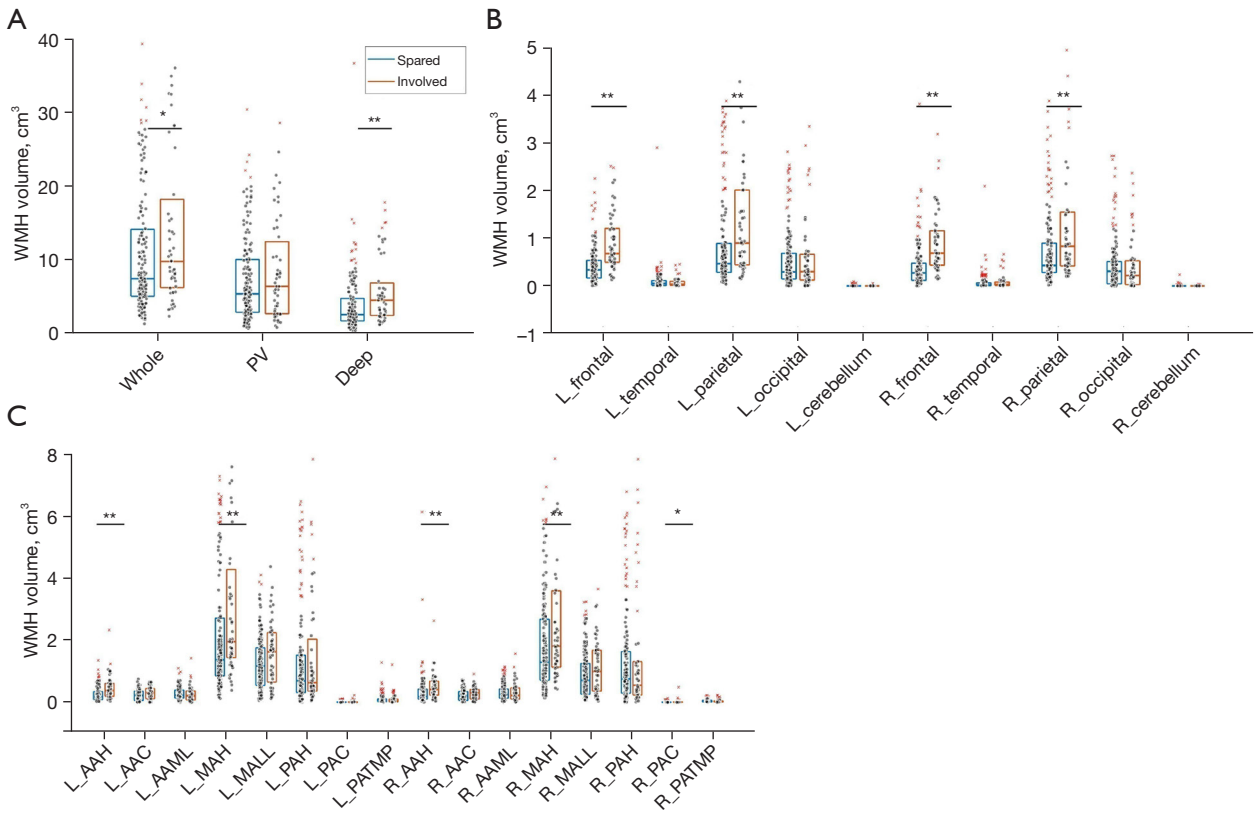

Figure 7 Differences in the volume of WMHs in different brain regions between the U-fiber-spared group and the U-fiber-involved group. Significant differences were marked by black asterisks (*) at the alpha significance level of 0.05. The double asterisks (**) represent a significant P value less than 0.01. (A) WMH volume comparison in whole white matter (Whole), periventricular (PV) and deep white matter (15). (B) WMH volume comparison in different lobes (bilateral frontal, temporal, parietal, occipital lobes) and cerebellum. (C) WMH volume comparison in different arterial territories. WMHs, white matter hyperintensities; L, left hemisphere; R, right hemisphere; AAH, anterior artery hemisphere; AAC, anterior artery callosal; AAML, anterior artery medial lenticulostriate; MAH, middle artery hemisphere; MALL, middle artery lateral lenticulostriate, PAH, posterior artery hemisphere; PAC, posterior artery callosal; PATMP, posterior artery thalamic and midbrain perforators.

surface reconstruction part), which will save a lot of time for future clinical applications. Moreover, our tool provides detailed visualization modules for clinicians to more intuitively interpret WMH volume and size, U-fiber cluster quantification features, and the relationship between WMH and U-fiber diffusion microstructure properties in WM lesions.

There have been several limitations in previous research on U-fibers. First, the tracking and filtering conditions of U-fibers are relatively simple, leading to the inclusion of pseudo-superficial fibers (60). In previous studies, U-fibers were filtered by 3 conditions (1): (I) the length of the fibers is usually between 20 and 80 mm (4); (II) the shape of the fiber usually satisfies $L/D \geq \pi$, where L is the arc length and D is the chord length (13), such condition specified the shape of the fibers to be U-shaped; (III) the U-fibers are in the ipsilateral hemisphere (2), and the superficial fiber connections of the corpus callosum are removed by coordinate screening. Unfortunately, most of these studies confused the concept of U-fibers with superficial fibers because they ignored the anatomical properties that U-fibers travel around the sulcus and connect adjacent gyri (60,61). Although a recent study considered the anatomical constraint that the origin and destination of the U-fibers are both in adjacent gyri (27), there remained a lack of an open-source toolbox for U-fibers tractography that is suitable for clinical research. We have provided a user-friendly multimodal MRI analysis tool truly designed for clinical applications. On the one hand, it can help clinicians to better utilize advanced MRI techniques, and on the other

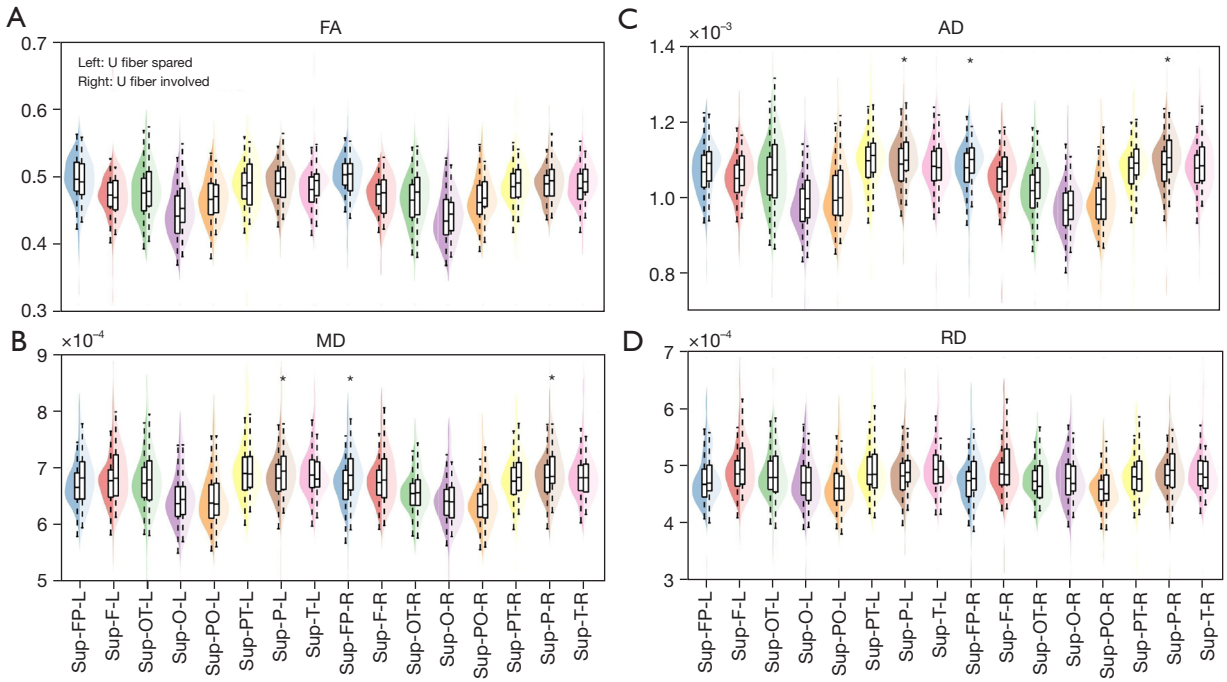

Figure 8 Differences in the U-fiber diffusion measures in different brain regions between the U-fiber-spared group and the U-fiber-involved group. Significant differences are marked by black asterisks (*) at the alpha significance level of 0.05. (A) FA; (B) MD; (C) AD; (D) RD. FA, fractional anisotropy; MD, mean diffusivity; AD, axial diffusivity; RD, radial diffusivity; L, left hemisphere; R, right hemisphere; Sup-FP, superficial-frontal-parietal; Sup-F, superficial-frontal; Sup-OT, superficial-occipital-temporal; Sup-O, superficial-occipital; Sup-PO, superficial-parietal-occipital; Sup-PT, superficial-parietal-temporal; Sup-P, superficial-parietal; Sup-T, superficial-temporal.

hand, it can promote algorithm researchers to focus on solving clinical practical problems.

Recent research has shown that the key to various brain functions lies in the connections and communication between different regions. Behavior and cognition also arise from the interaction between cortical areas (62). Therefore, U-fibers may play an important role in this process. U-fibers connecting different gyral regions may have different behavioral and cognitive functions. With the Destrieux atlas provided by FreeSurfer (55), UFA can obtain a segmentation of 82 U-fiber bundles. The analysis of U-fibers in different regions will help us to have a deeper understanding of the connection between brain regions and cognition. Moreover, different WM diseases have specific WM lesion regions, such as WMH of temporal polar in CADASIL (63), WMH of the trigeminal area in adrenoleukodystrophy (64), and extensive WMH of the frontal area in Alexander's disease (65). Therefore, the presence of U-fiber damage in specific brain regions may help us better understand the etiologies of these diseases.

There are few pieces of literature on the quantitative research of U-fiber, and those available have only investigated changes in the density and quantity of U-fibers or the changes in the network properties of the U-fibers (13,66). These indicators are relatively simple and cannot really help us understand how different MRI properties of the fibers are associated with different WM diseases. Our toolbox not only provides the description of microstructure diffusion metrics (FA/MD/AD/RD) of the U-fibers but also gives the WMHs volume and size in different brain regions for each patient with WM disease. It provides a detailed quantification tool to deeply understand the relationship between WMHs and U-fibers for WM disease.

Due to the late development of U-fibers, they are susceptible to damage in demyelinating diseases, such as multiple sclerosis (47). Moreover, the quantified diffusion parameters can reflect the damage of U-fiber earlier than WMHs (67). In an early-stage multiple sclerosis diffusion MRI study, Wu *et al.* (68) found that the diffusion properties of short-range fibers (e.g., U-fibers) were more severely affected than those of long-range fibers, which inspired us to focus on the U-fibers properties in early WM

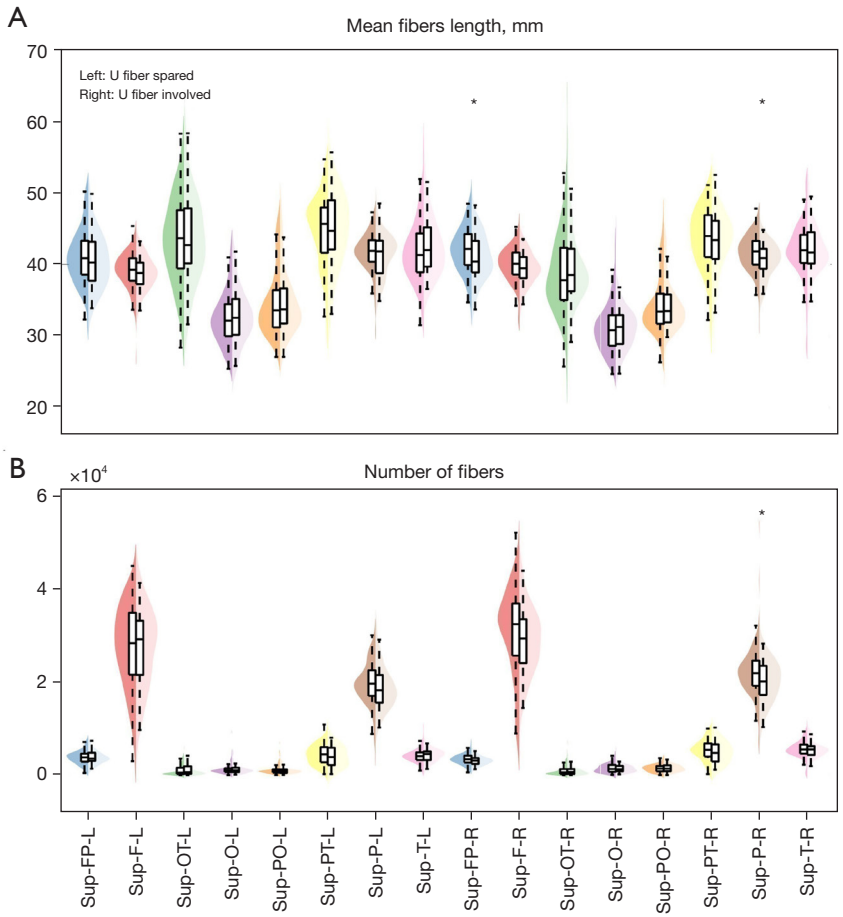

Figure 9 Differences in the macrostructural characteristics in different brain regions between the U-fiber spared group and the U-fiber involved group. (A) Mean fiber length of U-fibers; (B) number of U-fibers. Significant differences are marked by black asterisks (*) at the alpha significance level of 0.05. L, left hemisphere; R, right hemisphere; Sup-FP, superficial-frontal-parietal; Sup-F, superficial-frontal; Sup-OT, superficial-occipital-temporal; Sup-O, superficial-occipital; Sup-PO, superficial-parietal-occipital; Sup-PT, superficial-parietal-temporal; Sup-P, superficial-parietal; Sup-T, superficial-temporal.

disease. Meanwhile, a study of focal cortical dysplasia found that the U-fibers may play a role as a chemical barrier to the invasion of the heterotopic neurons from the DWM (69,70). All the evidence suggests that UFA is of great value in the early detection and diagnosis of the disease in the WM and at the grey-white matter junction. In this paper, we compared WMHs volume, cluster size, U-fiber diffusion parameters (FA/MD/AD/RD), fiber length, and the number of U-fibers in the groups with and without WMH-mediated U-fiber damages, and found that compared with the U-fiber-spared group (WMHs far away from U-fibers), the U-fiber-involved group (WMHs near the U-fibers) showed higher WMH burden in whole WM and DWM, especially in the frontal and parietal lobes. Moreover, we found that the U-fiber-involved group demonstrated more affected diffusion properties (AD/MD) in the parietal regions. We infer that the WMHs in the superficial layers would affect the microstructure of U-fibers. In the future, we will find out exactly how WMHs affect the microstructural properties of U-fibers and whether such association is affected by aging and other lesions (71).

It is important to note that the total running time of the UFA pipeline is still too long for clinical situations, although we already adopted the accelerated module by using GPU and CUDA. Here, we would like to emphasize that the currently developed UFA toolbox is still a basic version. In the future, we will further optimize the pipeline to accelerate the processes. Moreover, we will add more

useful functionalities, such as the analysis along U-fibers, the analysis of cortical thickness, and the calculation of gray matter and WM volume. Another limitation of this study is that the effect of WM lesions on the accuracy of fiber tracking was not assessed. Previous study has shown that FA values are typically lower in regions of WM damage than in normal WM and that errors are more likely to occur when the fiber tracking begins or ends in regions of WM damage (72). Besides, since the U-fibers are located in the superficial WM, the complex structures of gyri and sulci lead to the deviation between the results tracked by the algorithm and the actual anatomical U-fibers (73). We will explore more advanced tractography algorithms and validate the clinical value of our toolbox on large sample datasets from different scans/protocols (25,27,74).

Besides the long computation time, the UFA toolbox has some other shortcomings: for example, a lot of dependent packages (FSL, Freesurfer, FastSurfer, ANTs) need to be installed in advance to successfully use the UFA toolbox, which is a bit difficult for the clinical user. To compensate for this shortcoming, we have described in detail the process of installing the dependent packages in the user manual, as well as a series of problems that may occur when running the toolbox and their solutions. In addition, the UFA toolbox is currently limited to the Linux system, and in the future, we need to develop it to be compatible with the Windows or Mac operating systems so that cross-platform compatibility will be better.

Conclusions

We have developed a multi-modal neuroimaging analysis toolbox suitable for the analysis of U-fiber damage in cerebral WM disease. It provides an automated pre- and post-processing pipeline including tissue segmentation, WMHs extraction, and U-fiber tracking. The detailed visualization and quantification of WMHs and U-fibers can help us better observe whether WMHs affect the microstructural properties of U-fibers, which inspired them to understand the different disease mechanisms between those patients with and without U-fibers involvement.

Acknowledgments

We would like to thank Prof. Ye Wu of Nanjing University of Science and Technology for technical help with U-fiber tractography; PhD student Hongwei Li for help with diffusion MRI scanning of a healthy subject; PhD students Aiqi Sun, Shuai Xu, Bei Wang, Yuxiang Dai, Lixin Liu, and Prof. Chun-Yi Zac Lo for their selfless assistance during the development of the toolbox.

Funding: This work was supported by the project grants from Shanghai Municipal Committee of Science and Technology (No. 20Z11900800), the National Natural Science Foundation of China (No. 81971583), and the Shanghai Municipal Science and Technology Major Project (No. 2018SHZDZX01).

Footnote

Reporting Checklist: The authors have completed the STROBE reporting checklist. Available at https://qims.amegroups.com/article/view/10.21037/qims-23-847/rc

Conflicts of Interest: All authors have completed the ICMJE uniform disclosure form (available at https://qims.amegroups.com/article/view/10.21037/qims-23-847/coif). The authors have no conflicts of interest to declare.

Ethical Statement: The authors are accountable for all aspects of the work in ensuring that questions related to the accuracy or integrity of any part of the work are appropriately investigated and resolved. The study was conducted in accordance with the Declaration of Helsinki (as revised in 2013). The study was approved by the Ethics Committee of Zhongshan Hospital, Fudan University (No. B2018-155) and informed consent was provided by all individual participants.

References

1. Shastin D, Genc S, Parker GD, Koller K, Tax CM, Evans J, Hamandi K, Gray WP, Jones DK, Chamberland M. Short Association Fibre Tractography. bioRxiv 2021. doi: 10.1101/2021.05.07.443084.
2. Schüz A, Miller R. Cortical areas: unity and diversity.

London: CRC press; 2002.
3. Kirilina E, Helbling S, Morawski M, Pine K, Reimann K, Jankuhn S, Dinse J, Deistung A, Reichenbach JR, Trampel R, Geyer S, Müller L, Jakubowski N, Arendt T, Bazin PL, Weiskopf N. Superficial white matter imaging: Contrast mechanisms and whole-brain in vivo mapping. Sci Adv 2020;6:eaaz9281.
4. Gahm JK, Shi Y. Surface-based Tracking of U-fibers in the Superficial White Matter. Med Image Comput Comput Assist Interv 2019;11766:538-46.
5. Movahedian Attar F, Kirilina E, Haenelt D, Pine KJ, Trampel R, Edwards LJ, Weiskopf N. Mapping Short Association Fibers in the Early Cortical Visual Processing Stream Using In Vivo Diffusion Tractography. Cereb Cortex 2020;30:4496-514.
6. Pantoni L, Garcia JH. Pathogenesis of leukoaraiosis: a review. Stroke 1997;28:652-9.
7. De Reuck J, Santens P, Strijckmans K, Lemahieu I; European Task Force on Age-Related White Matter Changes. Cobalt-55 positron emission tomography in vascular dementia: significance of white matter changes. J Neurol Sci 2001;193:1-6.
8. Yoshino M, Saito K, Kawasaki K, Horiike T, Shinmyo Y, Kawasaki H. The origin and development of subcortical U-fibers in gyrencephalic ferrets. Mol Brain 2020;13:37.
9. Schüz A, Braitenberg V. The human cortical white matter: quantitative aspects of cortico-cortical long-range connectivity. In: Schuez A, Miller R, editors. Cortical areas: Unity and diversity. London: CRC press; 2002:377-85.
10. Schmahmann JD, Pandya DN. Fiber pathways of the brain. OUP USA; 2009. Available online: https://doi.org/10.1093/acprof:oso/9780195104233.001.0001
11. Barkhof F, Koeller KK. Demyelinating Diseases of the CNS (Brain and Spine). 2020.
12. Riley K, O'Neill D, Kralik S. Subcortical U-fibers: signposts to the diagnosis of white matter disease. Neurographics 2018;8:234-43.
13. O'Halloran R, Feldman R, Marcuse L, Fields M, Delman B, Frangou S, Balchandani P. A method for u-fiber quantification from 7T diffusion-weighted MRI data tested in subjects with non-lesional focal epilepsy. Neuroreport 2017;28:457.
14. Hau J, Aljawad S, Baggett N, Fishman I, Carper RA, Müller RA. The cingulum and cingulate U-fibers in children and adolescents with autism spectrum disorders. Human Brain Mapping 2019;40:3153-64.
15. Hau J, Baker A, Chaaban C, Kohli JS, Jao Keehn RJ, Linke AC, Mash LE, Wilkinson M, Kinnear MK, Müller RA, Carper RA. Reduced asymmetry of the hand knob area and decreased sensorimotor u-fiber connectivity in middle-aged adults with autism. Cortex 2022;153:110-25.
16. Kai J, Mackinley M, Khan AR, Palaniyappan L. Aberrant frontal lobe "U"-shaped association fibers in first-episode schizophrenia: A 7-Tesla Diffusion Imaging Study. NeuroImage: Clinical 2023;38:103367.
17. Jeurissen B, Descoteaux M, Mori S, Leemans A. Diffusion MRI fiber tractography of the brain. NMR Biomed 2019;32:e3785.
18. Guevara M, Román C, Houenou J, Duclap D, Poupon C, Mangin JF, Guevara P. Reproducibility of superficial white matter tracts using diffusion-weighted imaging tractography. Neuroimage 2017;147:703-25.
19. Guevara M, Guevara P, Román C, Mangin JF. Superficial white matter: A review on the dMRI analysis methods and applications. Neuroimage 2020;212:116673.
20. Reveley C, Seth AK, Pierpaoli C, Silva AC, Yu D, Saunders RC, Leopold DA, Ye FQ. Superficial white matter fiber systems impede detection of long-range cortical connections in diffusion MR tractography. Proc Natl Acad Sci U S A 2015;112:E2820-8.
21. Tournier JD, Calamante F, Gadian DG, Connelly A. Direct estimation of the fiber orientation density function from diffusion-weighted MRI data using spherical deconvolution. Neuroimage 2004;23:1176-85.
22. Tournier JD, Calamante F, Connelly A. Robust determination of the fibre orientation distribution in diffusion MRI: non-negativity constrained super-resolved spherical deconvolution. Neuroimage 2007;35:1459-72.
23. Tournier JD, Smith R, Raffelt D, Tabbara R, Dhollander T, Pietsch M, Christiaens D, Jeurissen B, Yeh CH, Connelly A. MRtrix3: A fast, flexible and open software framework for medical image processing and visualisation. Neuroimage 2019;202:116137.
24. Jeurissen B, Tournier JD, Dhollander T, Connelly A, Sijbers J. Multi-tissue constrained spherical deconvolution for improved analysis of multi-shell diffusion MRI data. Neuroimage 2014;103:411-26.
25. Wu Y, Hong Y, Feng Y, Shen D, Yap PT. Mitigating gyral bias in cortical tractography via asymmetric fiber orientation distributions. Med Image Anal 2020;59:101543.
26. Garyfallidis E, Brett M, Amirbekian B, Rokem A, van der Walt S, Descoteaux M, Nimmo-Smith I; . Dipy, a library for the analysis of diffusion MRI data. Front Neuroinform 2014;8:8.

27. Shastin D, Genc S, Parker GD, Koller K, Tax CMW, Evans J, Hamandi K, Gray WP, Jones DK, Chamberland M. Surface-based tracking for short association fibre tractography. Neuroimage 2022;260:119423.
28. Miki Y. Magnetic resonance imaging diagnosis of demyelinating diseases: An update. Clinical and Experimental Neuroimmunology 2019;10:32-48.
29. Zhang LJ, Tian DC, Yang L, Shi K, Liu Y, Wang Y, Shi FD. White matter disease derived from vascular and demyelinating origins. Stroke Vasc Neurol 2023. [Epub ahead of print]. doi: 10.1136/svn-2023-002791.
30. Weidauer S, Wagner M, Hattingen E. White Matter Lesions in Adults - a Differential Diagnostic Approach. Rofo 2020;192:1154-73.
31. Moody DM, Bell MA, Challa VR. Features of the cerebral vascular pattern that predict vulnerability to perfusion or oxygenation deficiency: an anatomic study. AJNR Am J Neuroradiol 1990;11:431-9.
32. Henschel L, Conjeti S, Estrada S, Diers K, Fischl B, Reuter M. FastSurfer - A fast and accurate deep learning based neuroimaging pipeline. Neuroimage 2020;219:117012.
33. Fazekas F, Chawluk JB, Alavi A, Hurtig HI, Zimmerman RA. MR signal abnormalities at 1.5 T in Alzheimer's dementia and normal aging. AJR Am J Roentgenol 1987;149:351-6.
34. Kellner E, Dhital B, Kiselev VG, Reisert M. Gibbs-ringing artifact removal based on local subvoxel-shifts. Magn Reson Med 2016;76:1574-81.
35. Avants BB, Tustison N, Song G. Advanced normalization tools (ANTS). Insight J 2009;2:1-35.
36. Hsu CH, Chong ST, Kung YC, Kuo KT, Huang CC, Lin CP. Integrated diffusion image operator (iDIO): A pipeline for automated configuration and processing of diffusion MRI data. Hum Brain Mapp 2023;44:2669-83.
37. Smith RE, Tournier JD, Calamante F, Connelly A. Anatomically-constrained tractography: improved diffusion MRI streamlines tractography through effective use of anatomical information. Neuroimage 2012;62:1924-38.
38. Veraart J, Novikov DS, Christiaens D, Ades-Aron B, Sijbers J, Fieremans E. Denoising of diffusion MRI using random matrix theory. Neuroimage 2016;142:394-406.
39. Andersson JLR, Sotiropoulos SN. An integrated approach to correction for off-resonance effects and subject movement in diffusion MR imaging. Neuroimage 2016;125:1063-78.
40. Skare S, Bammer R. Jacobian weighting of distortion corrected EPI data. Stockholm, Sweden 2010.
41. Andersson JL, Skare S, Ashburner J. How to correct susceptibility distortions in spin-echo echo-planar images: application to diffusion tensor imaging. Neuroimage 2003;20:870-88.
42. Andersson JLR, Graham MS, Zsoldos E, Sotiropoulos SN. Incorporating outlier detection and replacement into a non-parametric framework for movement and distortion correction of diffusion MR images. Neuroimage 2016;141:556-72.
43. Bastiani M, Cottaar M, Fitzgibbon SP, Suri S, Alfaro-Almagro F, Sotiropoulos SN, Jbabdi S, Andersson JLR. Automated quality control for within and between studies diffusion MRI data using a non-parametric framework for movement and distortion correction. Neuroimage 2019;184:801-12.
44. Jenkinson M, Beckmann CF, Behrens TE, Woolrich MW, Smith SM. FSL. Neuroimage 2012;62:782-90.
45. Smith SM, Jenkinson M, Woolrich MW, Beckmann CF, Behrens TE, Johansen-Berg H, Bannister PR, De Luca M, Drobnjak I, Flitney DE, Niazy RK, Saunders J, Vickers J, Zhang Y, De Stefano N, Brady JM, Matthews PM. Advances in functional and structural MR image analysis and implementation as FSL. Neuroimage 2004;23 Suppl 1:S208-19.
46. Greve DN, Fischl B. Accurate and robust brain image alignment using boundary-based registration. Neuroimage 2009;48:63-72.
47. Luo D, Peng Y, Zhu Q, Zheng Q, Luo Q, Han Y, Chen X, Li Y. U-fiber diffusion kurtosis and susceptibility characteristics in relapsing-remitting multiple sclerosis may be related to cognitive deficits and neurodegeneration. Eur Radiol 2023. [Epub ahead of print]. doi: 10.1007/s00330-023-10114-3.
48. Tournier JD, Calamante F, Connelly A, editors. Improved probabilistic streamlines tractography by 2nd order integration over fibre orientation distributions. Proceedings of the international society for magnetic resonance in medicine; 2010: John Wiley & Sons, Inc. New Jersey, USA.
49. Jiang J, Liu T, Zhu W, Koncz R, Liu H, Lee T, Sachdev PS, Wen W. UBO Detector - A cluster-based, fully automated pipeline for extracting white matter hyperintensities. Neuroimage 2018;174:539-49.
50. Wen W, Sachdev P. The topography of white matter hyperintensities on brain MRI in healthy 60- to 64-year-old individuals. Neuroimage 2004;22:144-54.
51. Jiang J, Paradise M, Liu T, Armstrong NJ, Zhu W, Kochan

NA, Brodaty H, Sachdev PS, Wen W. The association of regional white matter lesions with cognition in a community-based cohort of older individuals. Neuroimage Clin 2018;19:14-21.
52. Henschel L, Kügler D, Reuter M. FastSurferVINN: Building resolution-independence into deep learning segmentation methods-A solution for HighRes brain MRI. Neuroimage. 2022;251:118933.
53. Fischl B. FreeSurfer. Neuroimage 2012;62:774-81.
54. Schilling KG, Archer D, Yeh FC, Rheault F, Cai LY, Shafer A, Resnick SM, Hohman T, Jefferson A, Anderson AW, Kang H, Landman BA. Short superficial white matter and aging: a longitudinal multi-site study of 1293 subjects and 2711 sessions. Aging Brain 2023;3:100067.
55. Destrieux C, Fischl B, Dale A, Halgren E. Automatic parcellation of human cortical gyri and sulci using standard anatomical nomenclature. Neuroimage 2010;53:1-15.
56. O'Donnell LJ, Westin CF. Automatic tractography segmentation using a high-dimensional white matter atlas. IEEE Trans Med Imaging 2007;26:1562-75.
57. O'Donnell LJ, Wells WM 3rd, Golby AJ, Westin CF. Unbiased groupwise registration of white matter tractography. Med Image Comput Comput Assist Interv 2012;15:123-30.
58. Zhang F, Wu Y, Norton I, Rigolo L, Rathi Y, Makris N, O'Donnell LJ. An anatomically curated fiber clustering white matter atlas for consistent white matter tract parcellation across the lifespan. Neuroimage 2018;179:429-47.
59. Norton I, Essayed W, Zhang F, Pujol S, Yarmarkovich A, Golby AJ, Kindlmann G, Wassermann D, Estepar RSJ, Rathi Y, Pieper S, Kikinis R, Johnson HJ, Westin CF, O'Donnell LJ. SlicerDMRI: Open Source Diffusion MRI Software for Brain Cancer Research. Cancer Res 2017;77:e101-3.
60. Nie X, Shi Y. Probabilistic Tracking U-fiber on the Superficial White Matter Surface. bioRxiv 2022:2022.05.05.490829.
61. Oishi K, Huang H, Yoshioka T, Ying SH, Zee DS, Zilles K, Amunts K, Woods R, Toga AW, Pike GB, Rosa-Neto P, Evans AC, van Zijl PC, Mazziotta JC, Mori S. Superficially located white matter structures commonly seen in the human and the macaque brain with diffusion tensor imaging. Brain Connect 2011;1:37-47.
62. Thiebaut de Schotten M, Forkel SJ. The emergent properties of the connected brain. Science 2022;378:505-10.
63. Auer DP, Pütz B, Gössl C, Elbel G, Gasser T, Dichgans M. Differential lesion patterns in CADASIL and sporadic subcortical arteriosclerotic encephalopathy: MR imaging study with statistical parametric group comparison. Radiology 2001;218:443-51.
64. Bladowska J, Kulej D, Biel A, Zimny A, Kałwak K, Owoc-Lempach J, Porwolik J, Stradomska TJ, Zaleska-Dorobisz U, Sąsiadek MJ. The Role of MR Imaging in the Assessment of Clinical Outcomes in Children with X-Linked Adrenoleukodystrophy after Allogeneic Haematopoietic Stem Cell Transplantation. Pol J Radiol 2015;80:181-90.
65. Sosunov A, Olabarria M, Goldman JE. Alexander disease: an astrocytopathy that produces a leukodystrophy. Brain Pathol 2018;28:388-98.
66. Wilkinson M, Wang R, van der Kouwe A, Takahashi E. White and gray matter fiber pathways in autism spectrum disorder revealed by ex vivo diffusion MR tractography. Brain Behav 2016;6:e00483.
67. Yu WY, Xu Z, Lee HY, Tokumaru A, Tan JMM, Ng A, Murayama S, Lim CCT. Identifying patients with neuronal intranuclear inclusion disease in Singapore using characteristic diffusion-weighted MR images. Neuroradiology 2019;61:1281-90.
68. Wu H, Sun C, Huang X, Wei R, Li Z, Ke D, Bai R, Liang H. Short-Range Structural Connections Are More Severely Damaged in Early-Stage MS. AJNR Am J Neuroradiol 2022;43:361-7.
69. Sarnat HB, Hader W, Flores-Sarnat L, Bello-Espinosa L. Synaptic plexi of U-fibre layer beneath focal cortical dysplasias: Role in epileptic networks. Clin Neuropathol 2018;37:262-76.
70. Sarnat HB. Proteoglycan (Keratan Sulfate) Barrier in Developing Human Forebrain Isolates Cortical Epileptic Networks From Deep Heterotopia, Insulates Axonal Fascicles, and Explains Why Axosomatic Synapses Are Inhibitory. J Neuropathol Exp Neurol 2019;78:1147-59.
71. Wang S, Zhang F, Huang P, Hong H, Jiaerken Y, Yu X, Zhang R, Zeng Q, Zhang Y, Kikinis R, Rathi Y, Makris N, Lou M, Pasternak O, Zhang M, O'Donnell LJ. Superficial white matter microstructure affects processing speed in cerebral small vessel disease. Hum Brain Mapp 2022;43:5310-25.
72. Theaud G, Dilharreguy B, Catheline G, Descotaux M, editors. Impact of white-matter hyperintensities on tractography. 25th Annual Meeting of the International Society for Magnetic Resonance in Medicine (ISMRM). Honolulu: International Society for Magnetic Resonance

in Medicine; 2017.
73. Schilling K, Gao Y, Janve V, Stepniewska I, Landman BA, Anderson AW. Confirmation of a gyral bias in diffusion MRI fiber tractography. Hum Brain Mapp 2018;39:1449-66.
74. Wu Y, Feng Y, Shen D, Yap PT. Penalized Geodesic Tractography for Mitigating Gyral Bias. Med Image Comput Comput Assist Interv 2018;11072:12-9.

Cite this article as: Zheng G, Fei B, Ge A, Liu Y, Liu Y, Yang Z, Chen Z, Wang X, Wang H, Ding J. U-fiber analysis: a toolbox for automated quantification of U-fibers and white matter hyperintensities. Quant Imaging Med Surg 2024;14(1):662-683. doi: 10.21037/qims-23-847

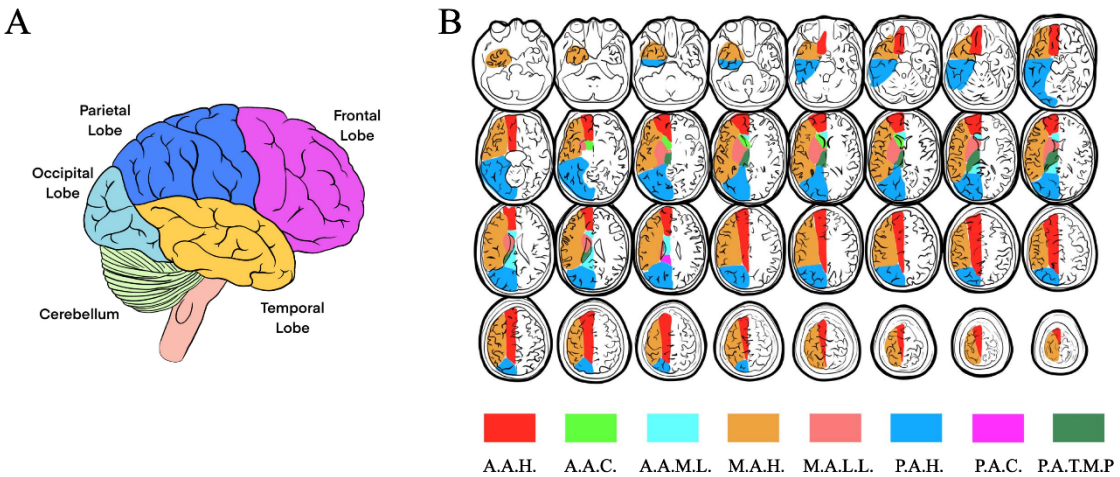

Figure S1 Schematic representation of (A) different lobes and (B) arterial regions in the white matter hyperintensity extraction section. It is worth noting that the panel B is a cartoon drawing with reference to Reference 1 (50). AAH, anterior artery hemisphere; AAC, anterior artery callosal; AAML, anterior artery medial lenticulostriate; MAH, middle artery hemisphere; MALL, middle artery lateral lenticulostriate, PAH, posterior artery hemisphere; PAC, posterior artery callosal; PATMP, posterior artery thalamic and midbrain perforators.

https://dx.doi.org/10.21037/qims-23-847

Table S1 The 82 paired neighboring gyri name were generated by using the Destrieux atlas (54)

No.	FreeSurfer-based nomenclature	FreeSurfer label number
1	ctx_lh_G_front_middle---ctx_lh_G_front_middle	11,115: 11,115
2	ctx_lh_G_front_sup---ctx_lh_G_and_S_cingul-Ant	11,116: 11,106
3	ctx_lh_G_front_sup---ctx_lh_G_front_middle	11,116: 11,115
4	ctx_lh_G_front_sup---ctx_lh_G_front_sup	11,116: 11,116
5	ctx_lh_G_precentral---ctx_lh_G_postcentral	11129: 11,128
6	ctx_lh_G_precentral---ctx_lh_G_precentral	11,129: 11,129
7	ctx_lh_S_central---ctx_lh_G_precentral	11,146: 11,129
8	ctx_lh_S_central---ctx_lh_S_central	11,146: 11,146
9	ctx_lh_S_front_inf---ctx_lh_G_front_middle	11,153: 11,115
10	ctx_lh_S_front_inf---ctx_lh_S_front_inf	11,153: 11,153
11	ctx_lh_S_front_middle---ctx_lh_G_front_middle	11,154: 11,115
12	ctx_lh_S_front_sup---ctx_lh_G_front_middle	11,155: 11,115
13	ctx_lh_S_front_sup---ctx_lh_G_front_sup	11,155: 11,116
14	ctx_lh_S_front_sup---ctx_lh_S_front_sup	11,155: 11,155
15	ctx_lh_S_orbital-H_Shaped---ctx_lh_S_orbital-H_Shaped	11,165: 11,165
16	ctx_lh_S_pericallosal---ctx_lh_G_front_sup	11,167: 11,116
17	ctx_lh_S_precentral-inf-part---ctx_lh_S_front_inf	11,169: 11,153
18	ctx_lh_S_precentral-inf-part---ctx_lh_S_precentral-inf-part	11,169: 11,169
19	ctx_lh_S_precentral-sup-part---ctx_lh_G_precentral	11,170: 11,129
20	ctx_lh_S_precentral-sup-part---ctx_lh_S_precentral-sup-part	11,170: 11,170
21	ctx_rh_G_front_middle---ctx_rh_G_front_middle	12,115: 12,115
22	ctx_rh_G_front_sup---ctx_rh_G_and_S_cingul-Ant	12,116: 12,106
23	ctx_rh_G_front_sup---ctx_rh_G_front_middle	12,116: 12,115
24	ctx_rh_G_front_sup---ctx_rh_G_front_sup	12,116: 12,116
25	ctx_rh_G_orbital---ctx_rh_G_orbital	12,124: 12,124
26	ctx_rh_G_precentral---ctx_rh_G_precentral	12,129: 12,129
27	ctx_rh_S_central---ctx_rh_G_precentral	12,146: 12,129
28	ctx_rh_S_front_inf---ctx_rh_G_front_middle	12,153: 12,115
29	ctx_rh_S_front_inf---ctx_rh_S_front_inf	12,153: 12,153
30	ctx_rh_S_front_middle---ctx_rh_G_front_middle	12,154: 12,115
31	ctx_rh_S_front_middle---ctx_rh_S_front_middle	12,154: 12,154
32	ctx_rh_S_front_sup---ctx_rh_G_front_middle	12,155: 12,115
33	ctx_rh_S_front_sup---ctx_rh_G_front_sup	12,155: 12,116
34	ctx_rh_S_front_sup---ctx_rh_S_front_sup	12,155: 12,155
35	ctx_rh_S_orbital-H_Shaped---ctx_rh_G_orbital	12,165: 12,124
36	ctx_rh_G_and_S_cingul-Mid-Post--ctx_rh_G_front_sup	12108: 12116
37	ctx_rh_S_precentral-inf-part---ctx_rh_S_front_inf	12,169: 12,153
38	ctx_rh_S_precentral-inf-part---ctx_rh_S_precentral-inf-part	12,169: 12,169
39	ctx_rh_S_precentral-sup-part---ctx_rh_G_precentral	12,170: 12,129
40	ctx_rh_S_precentral-sup-part---ctx_rh_S_precentral-sup-part	12,170: 12170
41	ctx_lh_G_pariet_inf-Angular---ctx_lh_G_pariet_inf-Angular	11,125: 11,125
42	ctx_lh_G_pariet_inf-Supramar---ctx_lh_G_pariet_inf-Supramar	11,126: 11,126
43	ctx_lh_G_parietal_sup---ctx_lh_G_parietal_sup	11,127: 11,127
44	ctx_lh_G_postcentral---ctx_lh_G_postcentral	11,128: 11,128
45	ctx_lh_S_intrapariet_and_P_trans---ctx_lh_G_pariet_inf-Angular	11,157: 11,125
46	ctx_lh_S_intrapariet_and_P_trans---ctx_lh_G_parietal_sup	11,157: 11,127
47	ctx_lh_S_intrapariet_and_P_trans---ctx_lh_S_intrapariet_and_P_trans	11,157: 11,157
48	ctx_lh_S_postcentral---ctx_lh_G_postcentral	11,168: 11,128
49	ctx_lh_S_postcentral---ctx_lh_S_postcentral	11,168: 11,168
50	ctx_rh_G_pariet_inf-Angular---ctx_rh_G_pariet_inf-Angular	12,125: 12,125
51	ctx_rh_G_pariet_inf-Supramar---ctx_rh_G_pariet_inf-Supramar	12,126: 12,126
52	ctx_rh_G_parietal_sup---ctx_rh_G_parietal_sup	12,127: 12,127
53	ctx_rh_Lat_Fis-post---ctx_rh_G_pariet_inf-Supramar	12,141: 12,126
54	ctx_rh_S_central---ctx_rh_S_central	12,146: 12,146
55	ctx_rh_S_intrapariet_and_P_trans---ctx_rh_G_pariet_inf-Angular	12,157: 12,125
56	ctx_rh_S_intrapariet_and_P_trans---ctx_rh_G_parietal_sup	12,157: 12,127
57	ctx_rh_S_intrapariet_and_P_trans---ctx_rh_S_intrapariet_and_P_trans	12,157: 12,157
58	ctx_rh_S_parieto_occipital---ctx_rh_S_parieto_occipital	12,166: 12,166
59	ctx_rh_S_postcentral---ctx_rh_G_postcentral	12,168: 12,128
60	ctx_rh_S_postcentral---ctx_rh_S_intrapariet_and_P_trans	12,168: 12,157
61	ctx_rh_S_postcentral---ctx_rh_S_postcentral	12,168: 12,168
62	ctx_lh_G_oc-temp_med-Lingual---ctx_lh_G_oc-temp_med-Lingual	11,122: 11,122
63	ctx_lh_S_oc_middle_and_Lunatus---ctx_lh_G_occipital_middle	11,158: 11,119
64	ctx_lh_S_oc_sup_and_transversal---ctx_lh_S_oc_sup_and_transversal	11,159: 11,159
65	ctx_lh_S_parieto_occipital---ctx_lh_S_parieto_occipital	11,166: 11,166
66	ctx_rh_G_cuneus---ctx_rh_G_cuneus	12,111: 12,111
67	ctx_rh_G_occipital_middle---ctx_rh_G_occipital_middle	12,119: 12,119
68	ctx_rh_G_oc-temp_med-Lingual---ctx_rh_G_oc-temp_med-Lingual	12,122: 12,122
69	ctx_rh_Pole_occipital---ctx_rh_Pole_occipital	12,143: 12,143
70	ctx_rh_S_oc_middle_and_Lunatus---ctx_rh_G_occipital_middle	12,158: 12,119
71	ctx_rh_S_oc_sup_and_transversal---ctx_rh_G_occipital_sup	12,159: 12,120
72	ctx_rh_S_oc_sup_and_transversal---ctx_rh_S_oc_sup_and_transversal	12,1259: 12,159
73	ctx_lh_S_temporal_sup---ctx_lh_G_pariet_inf-Angular	11,174: 11,125
74	ctx_lh_S_temporal_sup---ctx_lh_G_temporal_middle	11,174: 11,138
75	ctx_lh_S_temporal_sup---ctx_lh_S_temporal_sup	11,174: 11,174
76	ctx_rh_G_temporal_middle---ctx_rh_G_temporal_middle	12,138: 12,138
77	ctx_rh_Lat_Fis-post---ctx_rh_Lat_Fis-post	12,141: 12,141
78	ctx_rh_S_temporal_sup---ctx_rh_G_pariet_inf-Angular	12,174: 12,125
79	ctx_rh_S_temporal_sup---ctx_rh_G_temporal_middle	12,174: 12,138
80	ctx_rh_S_temporal_sup---ctx_rh_S_temporal_sup	12,174: 12,174
81	ctx_lh_G_and_S_cingul-Ant---ctx_lh_G_and_S_cingul-Ant	11,106: 11,106
82	ctx_rh_G_and_S_cingul-Ant---ctx_rh_G_and_S_cingul-Ant	12,106: 12,106

https://dx.doi.org/10.21037/qims-23-847

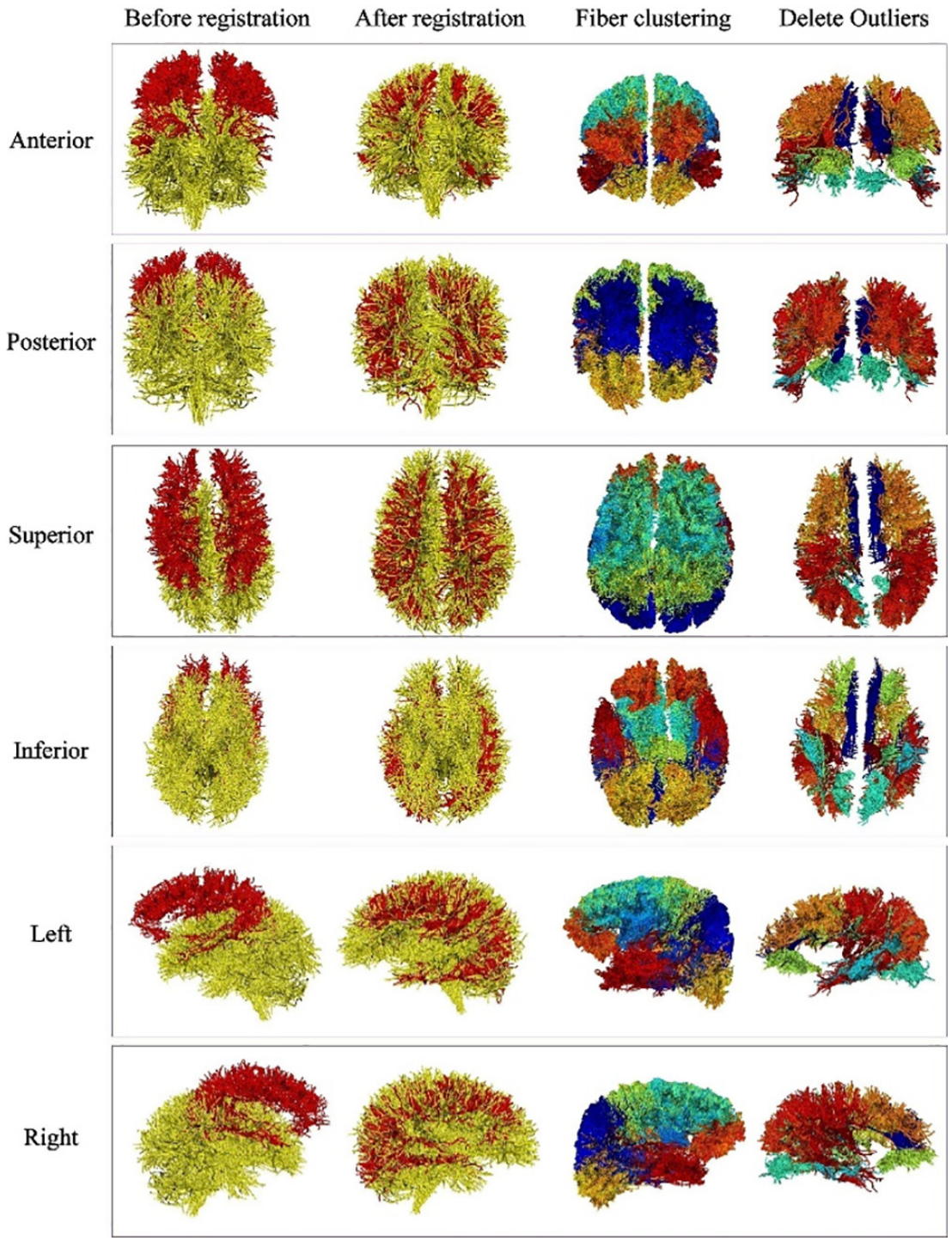

Figure S2 Visualization of U-fibers clustering from different views (anterior, posterior, superior, inferior, left, right). The U-fiber clustering process included the (I) registration of the white matter tractography to the atlas; (II) fiber clustering; and (III) outliers deleted.

https://dx.doi.org/10.21037/qims-23-847

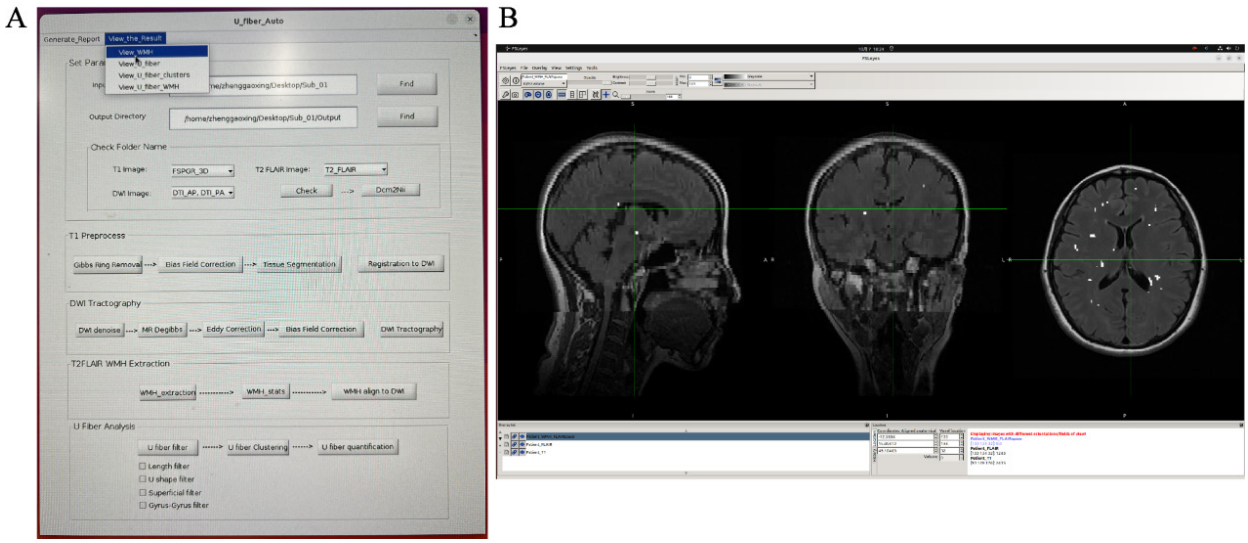

Figure S3 WMHs visualization module provided by UFA toolbox. (A) Shows the interface of the UFA toolbox, where the menu bar "View_the_Result" is the visualization module of UFA, and the drop-down menu "View_WMH" is the visualization module of WMHs, and the results in Figure B can be obtained by clicking "View_WMH"; (B) shows the WMHs extraction results of a subject, where the white dots indicate the automatically extracted WMHs. WMHs, white matter hyperintensities.

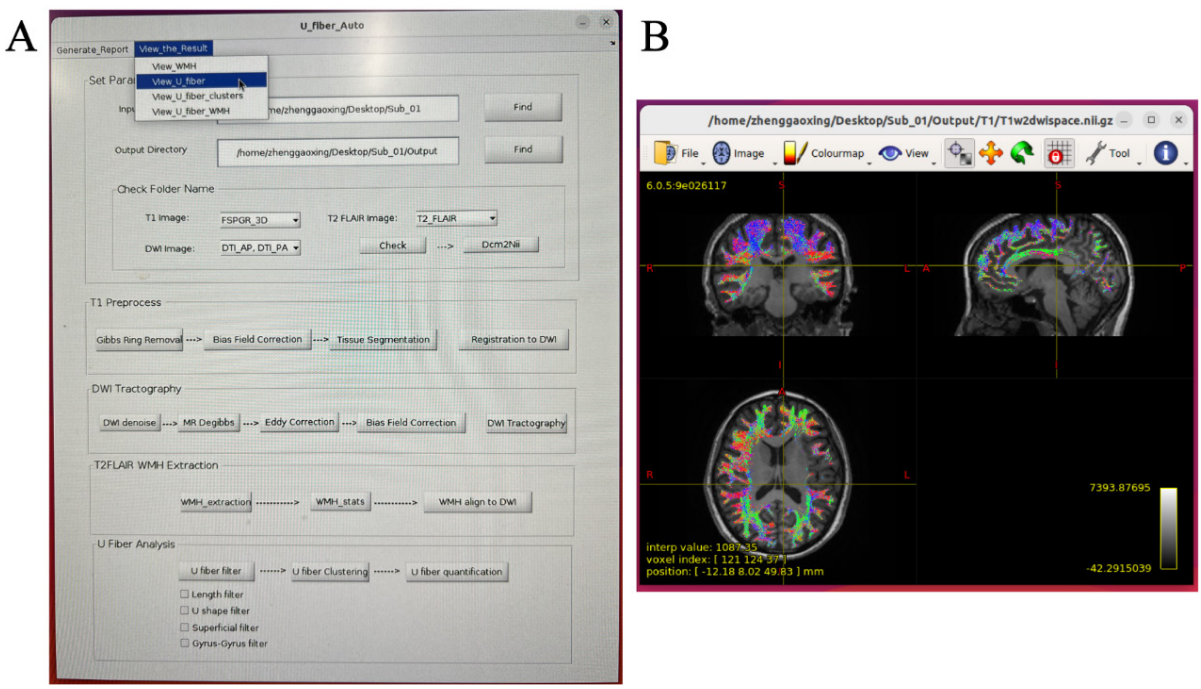

Figure S4 U-fibers visualization module provided by UFA toolbox.

https://dx.doi.org/10.21037/qims-23-847

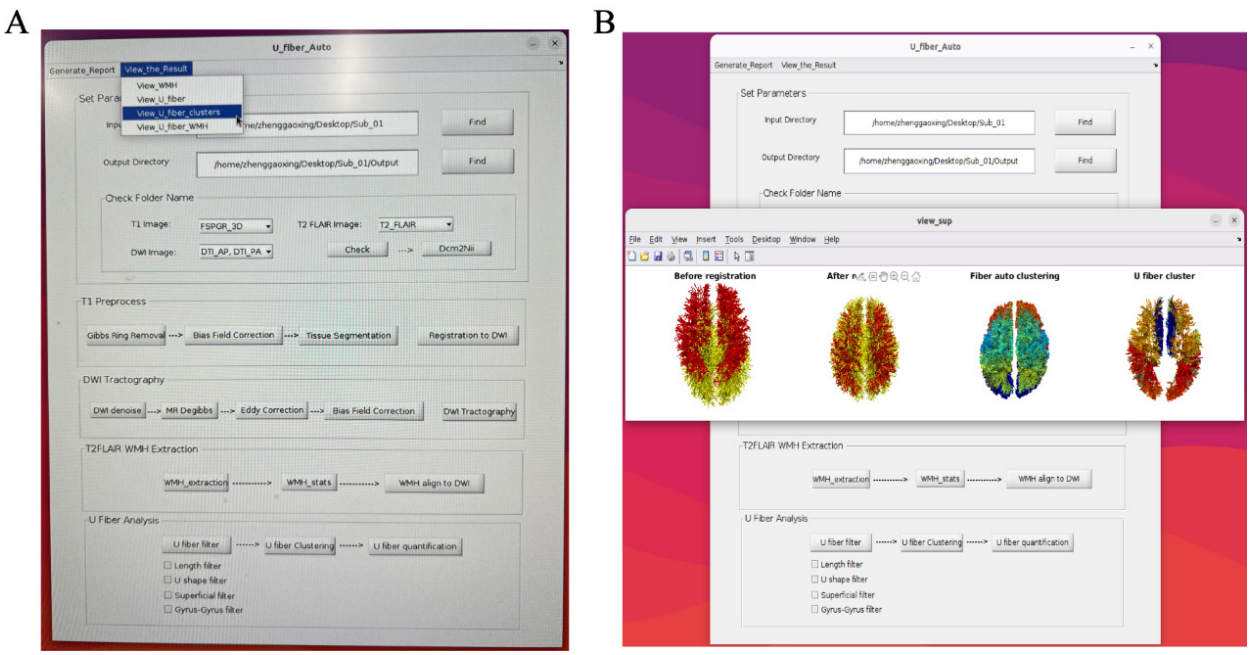

Figure S5 U-fiber clusters visualization module provided by UFA toolbox.

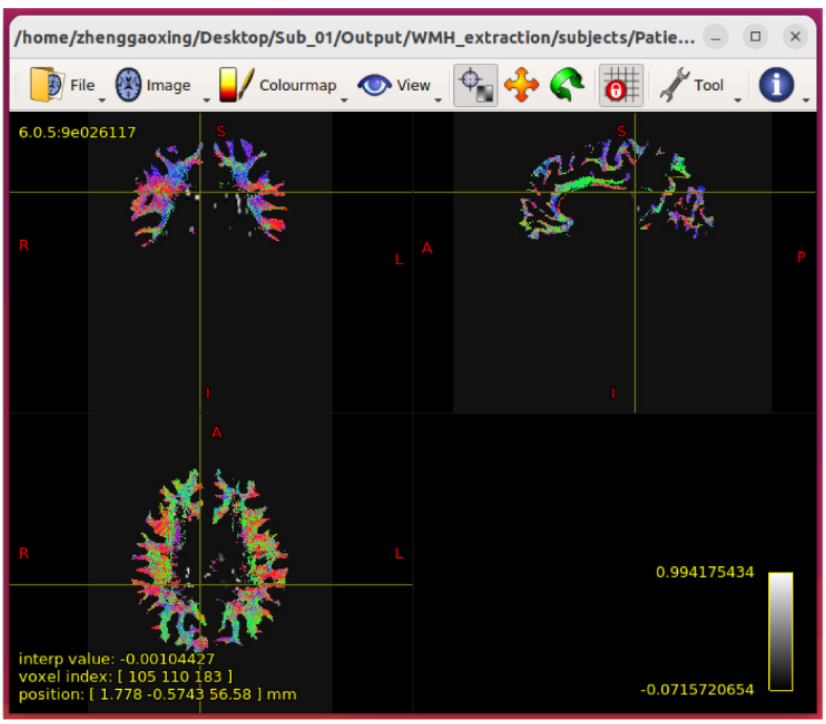

Figure S6 Visualization of WMHs and U-fibers overlapping together. The colored part is U-fibers, and the white dots are WMHs. Users can slide the mouse to see whether WMHs of different layers are attached to U-fibers. WMHs, white matter hyperintensities.

https://dx.doi.org/10.21037/qims-23-847

Figure S7 Neuroimaging analysis report automatically generated by the UFA toolbox. The title of the report is "The multi-modal neuroimaging report", and the first part is the basic information of the patient, such as "Name", "ID", "Gender", "Age", "Weight (kg)", "Birth Date", "Scan Time", "Modality". The second part is the volume and number of WMHs in different brain regions, including whole brain, PV and deep brain, as well as different brain lobes and arteries. The third part is the U-fiber quantification characteristics, including the number of the U-fiber, mean U-fiber length and the microstructural characteristics (AD/FA/MD/RD) of the U-fibers. WMHs, white matter hyperintensities; PV, periventricular; L, left hemisphere; R, right hemisphere; AAH, anterior artery hemisphere; AAC, anterior artery callosal; AAML, anterior artery medial lenticulostriate; MAH, middle artery hemisphere; MALL, middle artery lateral lenticulostriate, PAH, posterior artery hemisphere; PAC, posterior artery callosal; PATMP, posterior artery thalamic and midbrain perforators; FA, fractional anisotropy; MD, mean diffusivity; AD, axial diffusivity; RD, radial diffusivity; Sup-FP, superficial-frontal-parietal; Sup-F, superficial-frontal; Sup-OT, superficial-occipital-temporal; Sup-O, superficial-occipital; Sup-PO, superficial-parietal-occipital; Sup-PT, superficial-parietal-temporal; Sup-P, superficial-parietal; Sup-T, superficial-temporal.

https://dx.doi.org/10.21037/qims-23-847